Rainfall measurement from Commercial microwave links for urban hydrology in Africa: a simulation framework for sensitivity analysis.

Maxime Turko, Marielle Gosset, Modeste Kacou, Christophe Bouvier, Nanée Chahinian, Aaron Boone, Matias Alcoba

Revised R2 version - AMS Journal of HydroMeteorology - JHM-D-20-0163

Title Page:

Rainfall measurement from Commercial microwave links for urban hydrology in Africa: a simulation framework for sensitivity analysis.

Maxime Turko (1), Marielle Gosset (1), Modeste Kacou (2), Christophe Bouvier (3), Nanee Chahinian (3), Aaron Boone (4), Matias Alcoba (1).

1 -GET (IRD;CNRS;Université Toulouse III;CNES) , Toulouse, France

2- LAPA-MF (UFHB), Abidjan, Cote d'Ivoire

3-HSM (CNRS-IRD-UM), Montpellier, France

4-CNRM (Météo-France; CNRS), Toulouse, France

Corresponding author: marielle.gosset@ird.fr

Early Online Release: This preliminary version has been accepted for publication in *Journal of Hydrometeorology,* may be fully cited, and has been assigned DOI 10.1175/JHM-D-20-0163.1. The final typeset copyedited article will replace the EOR at the above DOI when it is published.

Abstract (<= 250 words)

Urban floods due to intense precipitation are a major problem in many tropical regions as in Africa. Rainfall measurement using microwave links from cellular communication networks has been proposed as a cost effective solution to monitor rainfall in these areas where the gauge network is scarce. The method consists in retrieving rainfall from the attenuation estimated along the commercial microwave links (CMLs) thanks to the power levels provided by an operator. In urban areas where the network is dense, rainfall can be estimated and mapped for hydrological prediction. Rainfall estimation from CMLs is subject to uncertainties. This paper analyzes the advantages and limitations of this rainfall data for a distributed hydrological model applied to an urban area. The case study is in West Africa in Ouagadougou where a hydrological model has been set up. The analysis is based on numerical simulations, using high resolution rain maps from a weather radar to emulate synthetic microwave links. Two sources of uncertainty in the rain estimation and on the simulated discharge are analyzed by simulations: i) the precision of the raw information provided by the operator and ii) the density and geometry of the network. A coarse precision (1 dB) in the signal provided by the operator can lead to substantial underestimation of rainfall and discharge, especially for links operating at low frequency (below 10 GHz) or short (less than 1 km). The density of the current mobile networks in urban areas is appropriate to analyze hydrological impact of tropical convective rainfall.

Accepted for publication in *Journal of Hydrometeorology*. DOI 10.1175/JHM-D-20-0163.1.

Main (< 7500 words)

1. Introduction

During the last 10 years, rainfall measurement from commercial microwave link (CML) network has gradually emerged as a useful complement to traditional rainfall measurement based on gauges, weather radar or satellites. Uijlenhoet et al. (2018) and Chwala and Kunstmann (2019) provide a good review of the state of the art and the research developed since the pioneering work of Messer et al. (2006) and Leijnse et al. (2007b)The CML technique is based on the analysis of attenuation induced by rain over the radio-frequency part of the mobile network, i.e. between pairs of telecommunication antennas. The main advantage of this technique is to exploit a network already in place and well maintained by mobile operators. In developing countries where the mobile network is already well developed (Noam 1999; ITU 2004) while hydro-meteorological services have limited resources (Novella and Thiaw 2013; Dieulin et al. 2019) the prospect for operational use of the CML technique is very appealing (Hoedjes et al. 2014; Gosset et al. 2016). The telecommunication network density follows population density (i.e. the customers) and most of the antennas lay in urban areas. This means that urban hydrology and urban flood risk monitoring is a subject area that could benefit from the CML technique (Fencl et al. 2013, 2015, 2017; Stransky et al. 2018; Pastorek et al. 2019). Cities in developing countries and especially in Africa are suffering from an increase exposure to extreme weather events (Bradshaw et al. 2007; Ebi and Bowen 2016; Egbinola et al. 2017; Engel et al. 2017). The amount of material damages and casualties due to flooding in West Africa has increased in the last decade under the conjunction of demographical pressure and population flow towards cities on one hand, and an increase of rainfall on the other hand. The mobile communication network could potentially contribute to a better monitoring of these hydrometeorological events. With current network

Accepted for publication in *Journal of Hydrometeorology*. DOI 10.1175/JHM-D-20-0163.1.

monitoring systems (NMS) or dedicated software CML rainfall is typically monitored at time steps of 5 to 15 minutes (Uijlenhoet et al. 2018; Chwala and Kunstmann 2019) which provides an interesting temporal resolution for urban hydrology. Data have been collected at even shorter time steps for some experiments (Schleiss and Berne 2010; Schleiss et al. 2013; Zinevich et al. 2009; Fencl et al. 2015; Chwala et al. 2016)

Most studies on CML estimation of rainfall have been based in European countries (Fenicia et al. 2012; Schleiss et al. 2013; Zohidov et al. 2016; D'Amico et al. 2016; Pastorek et al. 2019; de Vos et al. 2019; Polz et al. 2020; Graf et al. 2020; Roversi et al. 2020) and Israel (Messer et al. 2006; Zinevich et al. 2008, 2009). Most have focused on the quality of the estimate from this technique by comparison with rain gauges and/or weather radar. More recently, investigations on CML rainfall estimation have started outside Europe and Mediterranean countries (Hoedjes et al. 2014; Rios Gaona et al. 2017; Kim and Kwon 2018; Sohail Afzal et al. 2018). Doumounia et al. (2014) presented the first quantitative test of the technique in Africa, based on a single link.

A few studies discussed the interest of the CML rainfall for hydrological applications in Europe (Brauer et al. 2016; Smiatek et al. 2017) in particular for urban hydrology where the high spatial and temporal resolution of the rain maps is beneficial (Fencl et al. 2013, 2015, 2017; Stransky et al. 2018; Pastorek et al. 2019). These studies showed that the density of links in urban areas helps improving the simulation of the discharge dynamics compared to simulations based solely on rain gauges. They also pointed out some biases in CML rainfall estimate and their propagation in the simulated discharge. In african cities where the flood risk is very high and rainfall is due to intense convective systems, the CML technique seems particularly promising for urban hydrology. This study wishes to contribute to its development by analyzing the expected benefits.

The study by Doumounia et al. (2014) in Ouagadougou was part of the Megha-Tropiques satellite ground validation (MTGV) program (Gosset et al. 2018; Guilloteau et al. 2018). During this experiment a weather radar and a dense network of rain gauges were available. In order to take full

Accepted for publication in *Journal of Hydrometeorology*. DOI 10.1175/JHM-D-20-0163.1.

advantage of the CML-based rain maps when they will be available, the Institut de Recherche pour le Développement (IRD) started the development of a fully distributed hydrological model compatible with this urban context. Bouvier et al. (2017, 2018) have adapted their modeling platform ATHYS (ATelier en HYdrologie Spatialisée; Bouvier and Desbordes 1990; Bouvier et al. 2010) with a first validated set up for the city of Ouagadougou. The primary purpose of the present work is to investigate how such a distributed hydrological model can benefit from CML based rain estimation : what is the added value for hydrological prediction of the spatial information on rainfall provided by the CML network ; how does it balance with the uncertainties brought in by CML estimation ; what is the sensitivity of the predicted discharge to the CML network configuration. While CML and hydrological data is being gathered in various African test-beds (Cameroun; Niger), these questions are first investigated based on numerical simulations.

The proposed simulation framework is based on three components, i) the distributed hydrological model ATHYS, currently set up for the city of Ouagadougou, ii) high resolution (1 km; 5 minutes) rain maps acquired with a weather radar in Ouagadougou during the MTGV campaign ; these are the reference rain fields used for the reference hydrological simulations and to generate synthetic CML measurements, and iii) the production of pseudo-CML data simulated by positioning a virtual network inside the high resolution rain fields. With this set up several aspects of CML based rainfall measurement and uncertainty propagation into the model can be investigated.

There are many sources of uncertainty in rainfall estimation from a network of commercial microwave links (see Chwala and Kunstmann 2019 for a recent review). In this paper we primarily focus on two aspects that are directly linked to the network itself : i) the uncertainty in rainfall estimation at each individual link due to the inaccuracy of the raw signal (digitizing step) and the length and frequency of the link, and ii) the network spatial configuration and its capacity to represent rainfall characteristics over the basin.

Accepted for publication in *Journal of Hydrometeorology*. DOI 10.1175/JHM-D-20-0163.1.

Section 2 provides an introduction to rainfall measurement from commercial microwave links (CMLs). Section 3 introduces the study area and the simulation set up, the high-resolution radar data used as input for the link simulations, the hydrological model ATHYS and the numerical experiments carried out. Section 4 presents the results from the numerical experiments, analyzing the impact of the precision in attenuation measurement and of the spatial configuration of the network inside the basins. For both topics, the impact is first analyzed on rainfall and then on the simulated discharge. Section 5 provides conclusions and perspectives.

2. Rainfall measurement from commercial microwave links: principle and known limitations

The fundamental quantity used for rainfall estimation from CMLs is the specific attenuation *k* (dB/km) due to the rainfall along the wave propagation path. Because both *k* and the rainfall intensity *R* (mm/h) depend on the rain drop size distribution (DSD), they are related, and their relationship can be expressed via a power law:

$$k = a\,R^b \qquad (1)$$

where *a* and *b* depend strongly on the frequency, the polarization and more mildly on other factors (DSD; temperature etc.).

Table 1 around here

Table 1 reports values of *a, b* for several frequencies typical of the range commonly used on operational mobile networks. The values of *a* and *b* were computed using the Mie scattering model (Mie 1908) and DSDs measured in West Africa (Moumouni et al. 2008).

Between the two ends of a CML of length *L* the total (or path integrated) attenuation PIA can be estimated by comparing the transmitted (Tx) and received (Rx) powers. In most cases the transmitted

signal Tx is constant and rainfall attenuation is detected through variations (drops in signal) of Rx compared to its *baseline* level (Overeem et al. 2011; Chwala et al. 2012; Chwala and Kunstmann 2019). The PIA is the integral of *k* along the path:

$$PIA = \int_0^L k(s)ds = \int_0^L a\,R(s)^b ds \quad (2)$$

For practical purpose Eq. (2) is simplified to relate the PIA to the mean rate along the link, <*R*> :

$$PIA = < k > \; L = a' \; < R >^{b'} \; L \quad (3)$$

Unless rainfall is uniformly distributed along the link, or the exponent b is equal to 1, a′, b′ in Equation (3) are different from a, b in Equation (2) (Leijnse et al. 2008, 2010). For the frequency range 18 to 40 GHz (where *b* is close to 1, see Table 1) using (a, b) in Eq. (3) leads to little error. For short frequencies (below 15 GHz) the parameters need to be adjusted to account for rainfall variability along the link and the nonlinearity of the relation. Doumounia et al. (2014) used radar data from Ouagadougou to analyze this effect for a 29 km link operating at 7 Ghz, and found an increase of 25% in the prefactor *a'* compared to *a*. Similar calculations for a 5 km link gives an average increase of 3.5 % at 6 GHz and 2% at 12 GHz, and about twice these values for a 10 km link. Our data set based on 1 km radar data is however not best suited to analyze the small scale structure of rainfall.

Based on Eq. (3) and assuming that the parameters *a'* and *b'* are known, the rainfall estimation ($\hat{R}$) is given by:

$$\hat{R} = [{}^{PIA}/_{a'L}]^{1/b'} \quad (4)$$

Equation 4 and the values of *a* and *b* reported in Table 1 show that the amount of PIA for a given mean rain rate increases with the frequency and with the link length. For a given increment in PIA the equivalent rain rate is lower for higher frequencies and longer links, as illustrated in Table 1; for short links operating at low frequency the rainfall detection threshold may be high especially if the signal accuracy is coarse (1 dB). In this case low rainfall intensities will not be detected. The accuracy in the power levels provided by the operator, and the length and operating frequency of the CMLs are

therefore primary factors to consider in rainfall estimation and to assess the expected errors. As discussed in previous work (Leijnse et al. 2008a,b, 2010; Zinevich et al. 2010) there are several other sources of uncertainty in CMLs based rainfall estimation. One difficulty arises from the existence of fluctuations in the received power (Rx) that are not related to rainfall along the path. Attenuation by water vapor and other gas, refraction or reflection of the beam, mis-alignment of the antennas, can create such fluctuations. Drift in the electronics associated with temperature changes can also cause signal variability. These phenomena complicate the estimation of the *baseline* level during the dry periods and may cause error in rainfall detection and estimation. During and after rainfall, another source of error is the attenuation caused by antenna wetting (Leijnse et al. 2007a; Overeem et al. 2011; Chwala and Kunstmann 2019; Fencl and Bares 2019) which may lead to overestimating rainfall. There is not a simple analytical formula to relate the attenuation due to antenna wetting (in dB) at a given frequency to the rain rate, and its evolution in time. Experimental (Ostrometzky and Eshel 2018; Islam and Tharek 2000; Kharadly and Ross 2001) or theoretical (Leijnse et al. 2008a) analysis, and discussion with telecommunication engineers reveal that it depends on many factors like the material the antenna cover is made off or local wind effects. Given this complexity antenna wetting is not included in our simulations.

3. Study area, data and simulation setup

a. Study area

The area of Ouagadougou (12.3° N; 1.5°W) in Burkina Faso was selected as an illustrative test bed for the present sensitivity study for several reasons. Ouagadougou is representative of african cities exposed to increased flood risk as illustrated by several recent extreme events (Engel et al. 2017). In addition, all the information needed for the simulations is available for this city: i) Ouagadougou hosted

Accepted for publication in *Journal of Hydrometeorology*. DOI 10.1175/JHM-D-20-0163.1.

the first quantitative experimentation in Africa of rainfall measurement based on CMLs. This experiment, presented in Doumounia et al. (2014) was based on a single link, rain gauges and used data from the radar presented in section 3.b. The operator provided meta-data on the network lay out (Figure 1) which has been included in some of our simulations ; ii) Doumounia et al. (2014) experiment was part of the larger Megha-Tropiques Ground Validation program (MTGV ; http://meghatropiques.ipsl.polytechnique.fr/the-ouagadougou-super-site/ ; Gosset et al. 2018; Guilloteau et al. 2018) during which a weather radar was deployed for 2 years, providing high-resolution rain maps (see section 3.b) representative of african squall lines iii) a distributed hydrological model, well suited for flood prediction at the scale of a city and setup to use spatially distributed rainfall information was developed and calibrated for Ouagadougou (Bouvier et al. 2018) as presented in section 3.c.

Figure 1 displays the domain used for simulations (1250 km^2) and the layout of the CML network used for some of our simulations. For this urban network (one of several in Ouagadougou where more than one cellular phone company operates) all 75 links operate at 13 Ghz, their lengths range from 0.3 to 26 km over the domain. In our experience this density and size distribution is quite typical of what is found in other african cities, but there is a variety among countries, operators and depending on when the network was installed. In Niamey in Niger or Douala in Cameroun where we work with another operator, the number of links available over the urban areas are respectively 190 and 227; with frequencies ranging from 8.5 GHz to 23 GHz and lengths from 0.16 km to 6.59 km. Discussion with technical teams reveals that these networks are evolving with a tendency towards higher frequencies in the future.

The urban part of Ouagadougou is seen in the center (grey) of Figure 1 and the basins that drain water into the city are displayed. The two basins where rainfall estimation and discharge simulation are analyzed are highlighted. Their two outlets are respectively outlet 1060 (drainage area 448 km^2) in the northern part of the city and outlet 1074 (drainage area 139 km^2) more south. In each basin smaller

189 sub-basins are also used for testing, with outlet Ri1 and Ri3 (drainage area resp. 84 km^2 and 193 km^2)
190 in the northern basin, and Sa1 (74 km^2) in the South.

191 **######. Fig 1 around here**

192

193 *b. High resolution rainfall maps* from weather radar

194 The main data as input to the simulations is high resolution rain maps from a weather radar located in
195 Ouagadougou in 2012 and 2013. The radar is an X-band polarimetric radar from which 5 minutes, 1
196 km^2 rain maps were produced using an algorithm based on the polarimetric specific differential phase
197 shift ($R\text{-}K_{dp}$) as in Matrosov (2010), Kacou (2014) and Koffi et al. (2014).

198 In Ouagadougou as in most West Africa the rainfall season is associated with organized convective
199 systems characterized by a front of convective cells followed by a stratiform trail (Moumouni et al.
200 2008; Depraetere et al. 2009; Alcoba et al. 2016) and propagating mostly westwards. Figure 2 displays
201 the rain maps over Ouagadougou while a convective system recorded by the radar on 2012 August 4th
202 is crossing the area. The front of heavy rainfall associated with the convection arrives first followed by
203 more widespread and lower rain rates. Altogether three rainfall events that lead to heavy
204 precipitations and were well sampled by the radar are used for the simulations. Figure 3 displays the
205 hyetogram (rain rate versus time) of these events and the frequency distribution of rain intensities.
206 The values are typical of African squall lines, with most of the rainfall accumulation due to the
207 convective front which lasts about one hour, and only 20 to 30% of the event accumulation due to the
208 stratiform trail that lasts several hours. The heavy convective rainfall, with peak intensities well above
209 50 mm/h is the main driver for the floods and needs to be monitored. The spread in the value of the
210 percentiles in Figure 3 illustrates the spatial variability of rainfall over the domain, especially during
211 the convective front. The ability of the CML network to capture this variability is crucial as discussed in
212 section 4.

Accepted for publication in *Journal of Hydrometeorology*. DOI 10.1175/JHM-D-20-0163.1.

213 **######. Fig 2 and Fig 3 around here**

214

215 *c. Simulation setup*

216 The objective of the simulations is to analyze the capacity of the CML network to reproduce the
217 characteristics of the rain field that are needed to simulate the discharge. The benchmark is the
218 hydrological model forced by the high-resolution radar rain maps; they provide the reference
219 simulation.

220 CML-like data, mimicking various network configurations are generated from the radar maps. The
221 quality of these synthetic-CML rainfall estimates is first compared with the original rainfall maps. Then
222 these rainfall estimates are used as forcing to the hydrological model, and the simulated discharges is
223 compared to the reference (i.e. the model forced by the high-resolution rain map).

224

225 1) CML SIMULATION FROM RADAR DATA

226 The CML simulation is based on calculating the interception between the links and the radar maps. The
227 lines in Figure 2 display simulated links with their colors representing the mean rainfall over the link
228 path.

229 For each radar image, the mean rainfall over each link R_{link} is computed as the weighted average of the
230 rain rates over all radar pixels intercepted by the link:

231 $$R_{link} = \frac{\sum_{i=1}^{n} l_i R_{pix_i}}{\sum_{i=1}^{n} l_i} \quad (5)$$

232

233 with n the number of radar pixels intercepted by the link, l_i is the length of link intercepted by the
234 pixel, R_{pix_i} the rain intensity on the radar pixel *i*, and the link length is $L = \sum_{i=1}^{n} l_i$.

Accepted for publication in *Journal of Hydrometeorology*. DOI 10.1175/JHM-D-20-0163.1.

Similarly, the PIA is calculated based on the specific attenuation of each pixel,

$$PIA_{link} = \sum_{i=1}^{n} l_i k_{pix_i} \quad (6)$$

where k_{pix_i} is related to R_{pix_i} through Eq. (1) with the parameters (*a, b)* suited for the frequency of the simulated link. The simulated PIA can be altered by adding a measurement noise or considering other sources of errors. A rounding error of 1 dB or 0.1 dB can be considered as in section 4.1 to account for the coarse precision of the raw data provided by the operator. The rainfall estimated from the link $\hat{R}_{link}$ is then computed using Eq. 4. A range of values of the coefficients (*a, b*) can be tested in Eq. 4 to account for the uncertainty in the k-R relationship.

From the principle above a variety of CML network configurations can be tested by varying the frequency, length, position and orientation of the links. Several sources of uncertainty can be included in the simulations.

2) HYDROLOGICAL MODEL

A distributed hydrological model is needed to analyze the impact of rainfall spatial variability and to assess the ability of the CML network to reproduce rainfall characteristics that are important for the hydrological response. This work concentrates only on sensitivity analysis, by comparing the simulated response for various rainfall forcing. The purpose is not to evaluate the model output against real discharge data as these were not available when the radar was operating. The model was however setup and compared with real data in some areas of Ouagadougou, using rain gauge data, as described in Bouvier et al. (2018). The model is based on the open source platform ATHYS (www.athys-soft.org ; Bouvier and Desbordes 1990; Bouvier et al. 2010). The model has been used for flood modeling in many areas, especially for small catchments. Recently Bouvier et al. (2018) proposed a version of the model suited for the analysis of urban floods in African cities. The motivation was to propose a distributed gridded model operating over the whole city, with small computation time allowing real-

Accepted for publication in *Journal of Hydrometeorology*. DOI 10.1175/JHM-D-20-0163.1.

time forecasting. ATHYS distributed event-based parsimonious model, with Soil Conservation Service Lag-and-Route (SCS-LR) formula for runoff production and propagation is well suited for these constraints. As detailed in Bouvier et al. (2018) the model was setup over a 1000 km2 domain which includes the city of Ouagadougou as represented in Figure 1. The hydrographic network was defined using the Advanced Spaceborne Thermal Emission and Reflection Radiometer (ASTER) elevation model. This defines the 'natural' network in the rural area while the flux is forced by the street layout provided by the OpenStreetMap (/www.openstreetmap.org) data base for the built areas. The runoff is calculated based on the SCS formulation on elementary grid cells of resolution 10 m, and then propagated through the connected grid cells downstream using a 'lag and route' formula. The velocity of propagation over a given grid cell is parameterized by the slope at this grid point and by the drainage area upstream that grid. This is a simplified version compared to Bouvier et al. (2018) who also considered hydraulic propagation (kinematic wave) in some parts of the network. Another simplification is that the SCS parameters are uniform for the whole area (the interception parameter S is equal to 100 mm, in the range used by Bouvier et al. 2018) as the purpose here is to analyze the relative impact of various rain products, rather than the discharge simulation itself.

In this study rainfall is provided each 5 minutes, either on the radar grid (1 km resolution) for the reference simulation, or at the position of the links (center of each link) when testing the various network configurations. Inside ATHYS, the rainfall is interpolated at each grid point based on the Thiessen polygons method (Thiessen 1911).

3) REFERENCE SIMULATION

The reference simulations are based on the model above with the high-resolution rainfall maps (1 km resolution; 5 minutes time step) as forcing. A reference simulation is provided for each 3 rainfall events displayed in Fig.3. The discharge is calculated in 1078 intermediary points within the simulated area. In the next sections the discharge sensitivity to the rain forcing is analyzed specifically at the outlets of

the two main basins in Fig.1 (1060 and 1074) and their sub-basins (Ri1, Ri3 and Sa1). Part of the northern basin (outlet 1060) lays in rural areas which are poorly observed by the telecommunication network (Fig 1), while the southern basin (outlet 1074) is located mostly in the urban area, thus better covered by the mobile network.

4. Analysis of CML Rainfall uncertainty and propagation in discharge simulation

The simulation framework is used in this section to analyze uncertainties in rainfall estimation based on CMLs and its impact on the hydrological simulations. The reference simulation is based on the full resolution (1 km) rain maps. Synthetic CML rainfall estimates are produced using the link simulations introduced in section 3c for several network configuration.

First the impact of the precision of the attenuation data provided by the operator is tested in section 4*a*. For this experiment the links are positioned and oriented as in Fig. 1 and the impact of the rounding error on attenuation (0.1 or 1 dB) is analyzed considering several frequencies and link lengths. The impact is first analyzed on the retrieved rainfall distribution and then on the simulated discharge over the 2 main outlets 1060 and 1074.

Section *4b* concentrates on the spatial configuration of the network and its ability to sample rainfall variability within the basin. As above the analysis is first focused on the uncertainty on rainfall estimation over the basins and then on the simulated discharge. Several sub-basins of various size and shape are used.

a. Impact of PIA rounding error

As discussed in section 2 (Table 1) the accuracy of rainfall estimation from Eq. 4 depends on the precision of the PIA measurement itself, on the frequency (through the parameters *a* and *b*) and on the link length *L*. The most recent network monitoring systems (NMS) provide Tx and Rx with 0.1 dB or better, but more basic NMS provide only 1dB precision (Leijnse et al. 2007b; Fencl et al. 2015; Kim and Kwon 2018). The relative effect of PIA precision is stronger for the lowest rain rate and sets the lower limit of rainfall detection. According to Table 1 for instance the theoretical limit of detection for a link of 1km operating at 12 GHz and with a coarse accuracy of 1 dB is 22 $mm.h^{-1}$; rainfall below this threshold cannot be measured with such a link. For the highest end of the rainfall spectra (and specially for intense convective rainfall as in Africa) the relative error due to PIA is low (Leijnse et al. 2008a).

In order to analyze the impact of PIA precision on rainfall and subsequently discharge simulation, synthetic CML networks with precision 1 or 0.1 dB, and a range of frequency and length are simulated.

1) NUMERICAL EXPERIMENT

For this experiment the links' center position and their orientation are those provided by the operator meta-data in Ouagadougou for the 75 links shown in Figure 1 but the links' length, operating frequency, and the PIA precision can be changed. Three link lengths: 1, 5 and 10 km; five frequencies: 6, 12, 18, 24 and 30 GHz; and two rounding errors on the PIA: 0.1 and 1 dB, are considered. For each experiment the network is homogenous (same length, frequency and precision for all links).

The values of *a* and *b* used to simulate the PIA and the estimated rainfall at each link are those from Table 1. The only source of uncertainty in the simulation is the rounding error of the PIA.

2) ANALYSIS OF THE ERRORS IN RAINFALL ESTIMATION

######. Fig 4 around here

Figure 4 illustrates the error in the frequency distribution of the rainfall rates due to the rounding error, for links of size 1 km and the indicated frequencies. The calculation is done considering all three rainfall events. The curves in Fig.4 show the mean rainfall accumulation per link and per event, as a function

of the rain intensity class. The blue line is for a link with perfect precision (where the retrieved rainfall is exactly the mean link rainfall as in Eq.5), the other curves show the degradation as function of precision (0.1 or 1 dB) for the various frequencies. Figure 4 is consistent with the numbers displayed in Table1. A 1 km long link operating at 6 GHz would miss a substantial amount of rainfall, because an intensity above 26 mm/h is needed to create a 0.1 dB shift in attenuation, and 150 mm/h to create a 1 dB shift. Fortunately, short links (common in urban areas) usually operate at higher frequency, and a 10 km long 6 GHz link would have better detection (cf Table 1). As expected from Table 1, the distribution of rain intensity is better reproduced for higher frequencies and for all frequencies the errors are relatively lower for higher rain rates. This last point is important when considering the impact of the highest rain rates on floods. For 1 dB precision the overall bias on the mean event rainfall is small (about 10 %) from frequency 24 GHz and above. For a precision of 0.1 dB all the frequencies from 12 GHz and above provide a good reproduction of the rain rates, with biases below 5 %. The rendering would be better for longer links (and worse for shorter links) following Eq. (4).

It is worth stressing again that our simulations do not account for the wet antenna effect. Antenna wetting would typically increase the measured PIA by about 1dB (this is indicative; the range of values reported in the literature and by engineers is wide), with a risk of overestimating rainfall and creating false alarms. The existence of this positive bias can in practice counterbalance (compensating errors) some of the negative bias due to missing low rain rates with a coarse precision. Other effects such as the non-linearity of the attenuation-rainfall relationship (as discussed in section 2) tend to add a positive bias for long links (above 5 km) and frequency below 15 GHz if they are not accounted for in the retrieval. The strength of this effect depends on the variability of rainfall at small scale. According to our tests (based on the present radar data, not shown) the resulting impact of non-linearity is negligible compared to 1 dB rounding error.

3) PROPAGATION OF THE ERRORS INTO THE SIMULATED DISCHARGE

Accepted for publication in *Journal of Hydrometeorology*. DOI 10.1175/JHM-D-20-0163.1.

356 **######. Fig 5 around here**

357 Figure 5 displays the discharge simulated by the model at the outlets 1060 and 1074 (Fig. 1), for the
358 2012/08/04 event. The black line is the reference simulation based on the high-resolution radar map.
359 The dark blue line is the simulation based on the CML (1 km length and position as in Fig. 1) with perfect
360 precision (no error on the rainfall retrieval over the link), and the other colors display the tests with
361 precision 0.1dB (left) or 1 dB (right),and frequencies 6,12,18,24 and 30 GHz as in Fig. 4. The difference
362 between the reference (black) and the links with no error (dark blue) reflects solely the impact of
363 rainfall sampling. This will be discussed further in the next section. The difference between the various
364 colors and the dark blue line is related to the signal precision and its impact on rainfall estimation over
365 the basin. Fig. 5 confirms what was seen in Fig. 4, rain rates below a given threshold are undetected if
366 the precision is coarse, especially for the lower frequencies. With a precision of 0.1 dB -except for the
367 unlikely case of 1 km/6GHz link- the discharge is well reproduced; a coarse precision of 1 dB has a
368 negative impact on the simulated discharge, especially for frequencies below 24 GHz.

369 The results are generalized in Figure 6 for all 3 events and several numerical experiments: 5
370 frequencies; 2 precision levels and 3 link lengths (1, 5 and 10 km). The time series of the discharge
371 simulated at outlets 1060 and 1074 for each network configuration is compared with the discharge
372 simulated with the high-resolution radar maps. The average over the three events of the following
373 statistics are displayed as a function of frequency/length/precision : the mean bias on the discharge,
374 the relative error on the peak discharge and Kling–Gupta efficiency (KGE; Gupta et al. 2009).

375 Because of the high value of the coefficient *a* (Eq. 4; Table 1) the frequency 30 GHz is mostly immune
376 to a lack of precision up to 1 dB, even for the shortest link length considered here, 1 km. For this
377 frequency all 3 scores are good. For frequencies in the range 12-24 GHz which is very common in
378 current mobile networks in urban areas, a precision better than 1 dB is needed to reproduce rainfall
379 and discharge satisfactorily. For short links (1 km) with coarse precision (1 dB) in this range, the loss of
380 small to medium rain rates means an underestimation of the discharge and its dynamic (also seen in

Accepted for publication in *Journal of Hydrometeorology*. DOI 10.1175/JHM-D-20-0163.1.

Figure 5), impacting all 3 scores. For lower frequencies (6 GHz) a lot of rainfall is undetected leading to a strong underestimation of the discharge, its peak and its dynamic, unless the precision is 0.1 dB or better, and the length above 5 km.

The horizontal lines in Figure 5 show the scores for the links with perfect precision, considering the retrieved rainfall is exactly the weighted average over the radar pixels (Eq. 5). In that case the difference with the reference simulation is due to the difference in spatial sampling. We note that this difference is higher for outlet 1060 than for outlet 1074; this is explained by the position of the links inside the basin as seen in Fig 1. The network is more homogeneous and denser for the southeastern basin (outlet 1074), though not perfect, while rainfall in the eastern part of the northern basin (outlet 1060) is poorly sampled. For the latter the mean and peak discharge are underestimated. The results are also impacted by the length of the links as expected given the spatial variability of the rain field within squall lines (Fig. 2 and 3). The next section analyses further the question of the network spatial layout and its capacity to capture rainfall characteristics within the basin.

######. Fig 6 around here

b. Impact of network spatial layout

The network overall geometry, which includes the length, the position and the orientation of the links, determines its ability to capture and quantify rainfall variability inside the basin. As discussed with Figures 2 and 3, the convective systems that bring rainfall in West Africa exhibit high space-time variability.

This section investigates the impact of the network geometry on rainfall QPE (quantitative precipitation estimate) over the basin, then on the simulated discharge. This is based on several numerical experiments, either with varying length, density, and random positions and orientations of the links inside the basins or using the actual network of 75 links (Fig1).

Accepted for publication in *Journal of Hydrometeorology*. DOI 10.1175/JHM-D-20-0163.1.

1) NUMERICAL EXPERIMENT

The effect of the network geometry is investigated for 3 sub-basins of size 74 to 193 km^2 with outlets marked Ri1, Ri3 and Sa1 in Figure 1. The number of links per basin (i.e. a link which center is inside the basin) *N* varies from 1 to 100. For each value of *N*, 10 experiments with random positions and orientations of the links are generated. For each of these link positions and orientations, 3 lengths (1, 5 and 10 km) are considered as in section 4. Altogether 410 synthetic network configurations are simulated for each 3 sub-basins. For each, the 3 rainfall events are sampled with the link simulator (3.c). In these experiments only the network geometry is investigated, no error is considered in the estimation of the mean rainfall intensity over each link, which is simply calculated as in Eq (5).

2) RAINFALL ESTIMATION AND VARIABILITY WITHIN THE BASIN

######. Fig 7 around here

Figure 7 illustrates the spatial variability of rainfall as captured by the link network. The rainfall time series is from the 2012/08/04 event (Fig. 2 and 3). The seventy-five links positions of Figure 1 are used, but a heterogenous network of length 1 km (top) or 10 km (bottom) is simulated. At every 5 minutes time step there is a subsequent spread among the links. The spread is slightly reduced for the 10 km long links because of a spatial smoothing effect.

######. Fig 8 around here

Figure 8 summarizes the ability of different network configurations to quantify the time evolution of the mean area rainfall, and the spatial variability inside a basin. This example is for the 2012/08/04 event and the sub-basin Ri3 (Fig.1). Four configurations are considered: 1 km (left) or 10 km (right) long links; 1 (green) or 10 (red) links. For each configuration ten realizations were done, with random positioning of the links (center position and orientation). The black line is for the high-resolution radar map. The extension of the vertical green/red lines in Figure 8 illustrates the uncertainty due to the random positioning of the links to sample a highly variable rain field, consistent with Fig.7. The

Accepted for publication in *Journal of Hydrometeorology*. DOI 10.1175/JHM-D-20-0163.1.

uncertainty on the areal mean rain intensity (top plots) is very high when only one link is available per basin (green), and much reduced for ten links (red). For the same number and position of links, the estimation of the areal mean is more robust with the 10 km than with the 1 km links, as the former provide a 'natural averaging' of the rain field. Rainfall variability inside the basin is important for the hydrological response. The bottom plots of Figure 8 display the time evolution of the standard deviation (*std*) of rainfall within the sub-basin. The *std* is calculated at each five minutes time steps, among ten links (red) or among the radar pixels (black). As for the mean areal rainfall, random sampling of a variable field creates an uncertainty in the estimation, as illustrated by the red spread. Over ten realizations, the estimate of the *std* is un-biased for the 1 km long links and underestimated for the 10 km long links. Figure 8 is only illustrative, the quantitative impact of the link density and size within a given basin and rainfall event varies according to the rain field structure and the basin hydrological response.

3) SIMULATED DISCHARGE

######. Fig 9 around here

Figure 9 illustrates the uncertainty in the simulated discharge due to the imperfect sampling of rainfall variability inside the basin. The simulated discharge is analyzed at Ri3; the tested network configurations are the same as for Figure 8a/c: ten realizations (various colors) of a network with ten links of length 1 km. The spread within the ten realizations is larger for the simulated discharge (Fig. 9) than for the mean rainfall (Fig 8a). For several random positions of the links the peak discharge is overestimated by a factor close to two; while for one of the simulations (set 1), the peak is underestimated by a factor 3 and not in phase. The enhanced sensitivity of the discharge simulation to the position of the links is explained by the impact of rainfall variability within the basin on the hydrological response. The reproduction of discharge sensitivity to the rainfall pattern is model-

dependent. The sensitivity is enhanced by the non-linearity of the model equations (SCS formula) and well perceived with a high-resolution distributed model like ATHYS.

######. Fig 10 around here

Figure 10 synthetizes the results for all the experiments with the randomly positioned network (3 link lengths x 10 realizations x 3 events X 3 sub-basins; Fig 10a, b) and with the actual network of 75 links (Fig 10c); for the latter, tests were made keeping all links, or only links up to 5 km length, or only links longer then 5 km. In order to summarizes the total length of links inside the basin for each configuration a link density [km/km^2] equal to the sum of the link lengths divided by the sub-basin area, is introduced. The KGE of the simulated discharge compared to the reference simulation is plotted against the link density. The numerical experiments with different link lengths are plotted in color (1 km, blue; 5 km green; 10 km, red). Figures 10a and b, based on the randomly distributed network, show that the quality of the hydrological simulations increases sharply with the density of information provided by the links. From about 0.5 km/km^2 (i.e. for instance, ten 5 km links in a basin of 100 km^2) all simulations have a positive KGE. The increase in the simulation quality is sharper and the KGE for a given density higher for short links, as the rain field structure is better sampled with several small links than a single long one. For instance, the mean KGE is above 0.5 for a density equivalent to ten 1 km link per 100 km^2 (density, 0.1), but five 5 km or two 10 km length 100 km^2 (density 0.25) are needed for the same scores. Fig. 10c provides a similar analysis for the real network configuration of 75 links seen in Fig. 1, with their lengths ranging from 0.3 to 26 km. As for the top figures the rainfall at each link is the weighted average (Eq. 5), no estimation error is considered. In order to compare the relative impacts of the shortest and longest links, the results are also presented, when only the 18 links longer than 5 km or on the contrary the 57 links shorter than 5 km, are kept. For link linear density below 0.5 (km/km^2) the spread for a given basin and network configuration (same shape and color) illustrates the variability of the rainfall structure among the 3 rain events. For

a given linear density (in km/km^2), event and basin there is no significant difference between the tests where we kept only the smallest (below 5km) or on the contrary the longest (above 5km) links. It is noteworthy that because of the Thiessen interpolation method, a link which is partially or entirely outside a sub-basin may or not contribute to the rain estimation for this basin and a given configuration, depending on the other links available. The differences between events and the impact of the configuration is marked for outlet Ri3 which is mostly rural and poorly sampled by the real network.

Figure 10 is illustrative. More case studies would be needed to account for the complexity of the problem and all the parameters to be considered like the orientation of the links compared to the anisotropy of the rain field, the spatial decorrelation of the rain field, the size and shape of the basin etc. Figure 10 and the other figures in this section tend to show that a dense (in km/km²) network of short links, if they are evenly spread inside the basin (not clustered), is more suited for hydrology than the same linear density of longer links, because it samples better rainfall variability inside the basin. As noted in section 3c the rain information is spatialized in ATHYS by considering each rainfall estimate as a punctual value at the center of the link and using Thiessen interpolation. Other interpolation methods (Zinevich et al. 2008, 2009) could be used to exploit the spatial information provided by the links and account for their length and orientation. This a field of research on its own. Capturing the spatial variability of rainfall is however only one aspect of the problem.

c. Discharge spatial distribution

#####. Fig 11 and Fig 12

Figures 11 and 12 illustrate the spatial variability of rainfall and of the simulated discharge quality. Figure 11 show the rainfall accumulation for the 2012/08/04 event as seen by the high-resolution radar map. A strong gradient is seen from North to South, and in several locations inside the city the rainfall accumulation is high, with the maximum value over the domain at 70 mm and a minimum at 7 mm. This is consistent with the strong variability observed at 5 minutes time steps in Figures 2 and 3. As

discussed previously, the CML network captures only partially this intense rainfall variability. Figure 12 analyses the ability of the model, forced by the CML network to represent the spatial variability of the discharge. The experiment is with the original network as seen in Figure 1, with all links operating at 13 GHz. The top left map is for precision 1 dB and the top right precision 0.1 dB. The values of the KGE of the simulated discharge compared to the reference (simulation with high resolution radar map) are mapped in different points within the basin. The simulation for a 0.1 dB precision is improved, but the simulation with 1dB is already satisfactory, with the KGE for most points within the basin above 0.4. To put the performance of the CML based simulations in perspective compared to other types of rainfall measurement, the bottom figures display the results for two extra experiments: for Fig 12c the sampling of a satellite rainfall product was emulated by averaging the high resolution radar rain maps over the whole domain (about 1000 km^2) – no error on the satellite estimation is considered which is a strong idealization; for Figure 12d the rainfall series used to force the hydrological model comes from the central pixel (white star) emulating what a single rain gauge situated in the city center would see. In most of the basin the simulations based on the CML sampling represent much better the discharge and its variability than the simulations based on a single source of information (spatial average or single gauge). This good results in the urban part of the basin are consistent with previous findings. Fencl et al. (2013, 2015) also found that the density of the network at urban scale is beneficial to reproduce the hydrological dynamics. They also notice that the links, especially when short, may introduce bias in the rainfall and recommend using both gauge and link information (Fencl et al. 2017; Smiatek et al. 2017). Similar conclusions were drawn by Pastorek et al. (2019) and Stransky et al. (2018). Only at the very East end of the basin, where only two long links are available, the simulation based on the central pixel or the average perform slightly better than the CML. The benefit of the CML sampling for distributed hydrological modeling, even when a coarse precision is considered in the raw signal, is clearly striking in Fig. 12. The results are very similar for the 2 other rainfall events. Table 2 summarizes the results of these experiments for the three events. The statistical scores for the discharge at two main basins outlets (1060 and 1074) are reported. The error on the mean and on the maximum

Accepted for publication in *Journal of Hydrometeorology*. DOI 10.1175/JHM-D-20-0163.1.

discharge are much lower for the links, even with coarse precision, than for the single pixel or spatial mean forcing. The benefit of the CML ability to capture rainfall is also marked on the KGE, confirming the importance of the spatial information on rainfall to reproduce the discharge dynamics. For both sub-basins the linear link density (defined in 5b) is above 0.4 km/km^2 and KGE above 0.7, even with coarse precision. The results are even better for outlet 1074, with KGE above 0.9 whatever the precision, because the network covers this basin more homogenously.

Table 2 around here

6. Conclusion

This work investigates the potential benefits of CMLs rainfall estimation for urban hydrology in West Africa. One expected benefit of CMLs for hydrological application is the density of the network, especially in urban, thus populated, areas; on the other hand, as for any indirect measurement, rainfall estimation from CMLs is subject to uncertainties. A pending question for the development of CMLs based hydrological applications is: what is the final balance between the benefits and drawbacks of CMLs rain measurements, and how basin dependent and network dependent are they.

A simulation setup based on high resolution radar rain maps and a distributed hydrological model was used for a case study over the city of Ouagadougou. The radar is a research radar that operated in Burkina Faso as part of a satellite validation program in 2012 and 2013. The distributed model (ATHYS) was developed and calibrated for Ouagadougou area in the framework of an urban flood prediction project. Here the radar rain maps were used as a reference rainfall, as forcing to the hydrological model and for generating synthetic CML measurements which can in turn be used as model input. This setup was used to analyze the ability of the microwave link network to i) quantify rainfall over the urban basins, ii) to capture rainfall space and time variability. In this work we primarily focused on two characteristics of the CMLs network that influence rainfall estimates: i) the accuracy of the raw

information (digitizing step) provided by the operator and ii) the network configuration that includes the position and orientation, length and operating frequency of the links.

For the majority of numerical experiments, the discharge simulated with the synthetic links data as entry is close to the reference based on the high-resolution radar map. The performance is reduced when the raw data from the operator is provided with a coarse precision (1dB), especially if the frequency is low (below 10 GHz) and for short links, because the lower rain rates are undetected. The trend in mobile communication networks is for the operating frequencies to increase in order to match the operational needs (need for increase bandwidth in particular), this will help the detection of rainfall from CMLs. Higher operating frequencies are also expected in the perspective of the next generation networks (5G). As the networks modernize the built in monitoring software are also improved and accessing to the data with a good sampling rate (15 minutes or less) and fine precision (0.1 dB) becomes common (personal communications from Orange and Nokia engineers). The number of links inside the basin is important. To quantify this effect, numerical experiments with an increasing number of links randomly distributed within the sub-basins were performed. The performance in terms of discharge dynamics (KGE criteria), mean bias and error on the maximum discharge increases quickly with the network density -expressed in total length of link in km per km^2 of basin- and especially with the number of short (1 km) links. For the present simulations satisfactory results (KGE close to or above 0.5) are obtained from a density of 0.1 km/km^2 for 1 km long links (i.e. 10 links inside a 100 km^2 basin) and 0.3 km/km^2 (3 links of size 10 km for 100 km^2). When the positions of a real network are used, with a total of seventy-five links of various lengths for the Ouagadougou area (1000 km^2) the simulations with the CML sampling are very close to the reference (KGE above 0.5) for most of the basin. The CML sampling, even when a coarse precision is considered, outperforms the simulation based on idealized satellite pixel or a single gauge situated in the city center.

These good results are partly explained by the nature of rainfall systems in the study region. Rainfall in West Africa (and in most of the Tropics) is provided by deep convection, where most of the rain

Accepted for publication in *Journal of Hydrometeorology*. DOI 10.1175/JHM-D-20-0163.1.

accumulation is associated with intense rain rates. These intense rain rates create a strong micro-wave attenuation which is well detected by the CML network, whatever the length and frequency. The present work and previous studies show indeed that the relative error on rainfall estimation from CML decreases with rainfall intensity (Leijnse et al. 2008a,b). The spatial organization and dynamics of the convective cells influence the space-time structure of the rain fields. The relevant observational scales to capture these structures are kilometric and sub-hourly, which is compatible with the current CML networks in populated areas.

This positive outcome encourages to continue promoting CMLs as a source of information on rainfall quantities and space-time distribution in urban basins, especially in tropical regions where weather radar is not yet routinely available.

The presented simulation setup could be used for further sensitivity studies and for accounting for other sources of uncertainties that were not explicitly considered here (wet antenna; error in the baseline determination; uncertainty in the attenuation-rain rate relationship etc.). Here only the errors brought in by the difference in the rain forcing were considered, by comparing the output to a reference simulation based on a high-resolution radar map and a given setup of the hydrological model. The radar data is used as a realistic proxy of rain fields for simulations purposes. In reality radar estimation of rainfall is subject to many uncertainties, described at length in the literature (Berne and Krajewski 2013; Cecinati et al. 2017). The hydrological brings in its own uncertainties in the discharge prediction system (Beven and Binley 1992; Ajami et al. 2007). They come from the simplistic representation of hydrological processes, the equifinality problem in the optimization of parameters and other factors such as the interpolation of the rain information inside the model. These were beyond the scope of this paper but are being investigated.

Accepted for publication in *Journal of Hydrometeorology*. DOI 10.1175/JHM-D-20-0163.1.

603

604

605

606 **Acknowledgments**

607 Maxime Turko's PhD was funded by the French Space Agency CNES and Meteo-France
608 CNRM. The radar experiment in Ouagadougou was financed by the French Space Agency
609 CNES as part of the Megha-Tropiques Ground Validation (MTGV) program. We would like
610 to thank Frédéric Cazenave who installed the radar and supervised its operation. We are very
611 thankful to the technical teams from telecommunication operators who have provided us with
612 meta-data and data from their networks in several african countries, in particular at Telecel
613 and Orange.

614 **Data Availability Statement**

615 The data used for this study is openly available – A specific repository will be created when
616 the paper is accepted.

617 ATHYS code is freely available here: http://www.athys-soft.org.

618 **References**

619 Ajami, N. K., Q. Duan, and S. Sorooshian, 2007: An integrated hydrologic Bayesian
620 multimodel combination framework: Confronting input, parameter, and model
621 structural uncertainty in hydrologic prediction: AN INTEGRATED BAYESIAN
622 MULTIMODEL FRAMEWORK. *Water Resour. Res.*, **43**, 19,
623 https://doi.org/10.1029/2005WR004745.

624 Alcoba, M., M. Gosset, M. Kacou, F. Cazenave, and E. Fontaine, 2016: Characterization of
625 Hydrometeors in Sahelian Convective Systems with an X-Band Radar and
626 Comparison with In Situ Measurements. Part II: A Simple Brightband Method to Infer
627 the Density of Icy Hydrometeors. *J. Appl. Meteorol. Climatol.*, **55**, 251–263,
628 https://doi.org/10.1175/JAMC-D-15-0014.1.

629 Berne, A., and W. F. Krajewski, 2013: Radar for hydrology: Unfulfilled promise or
630 unrecognized potential? *Adv. Water Resour.*, **51**, 357–366,
631 https://doi.org/10.1016/j.advwatres.2012.05.005.

632 Beven, K., and A. Binley, 1992: The future of distributed models: Model calibration and
633 uncertainty prediction. *Hydrol. Process.*, **6**, 279–298,
634 https://doi.org/10.1002/hyp.3360060305.

Bouvier, C., and M. Desbordes, 1990: Un modèle de ruissellement urbain pour les villes d'Afrique de l'Ouest. *Hydrol. Cont.*, **5**, 10.

Bouvier, C., A. Crespy, F. N. L'Aour-Dufour, F. Cres, F. Delclaux, and A. Marchandise, 2010: Modélisation hydrologique distribuée - Plate-forme ATHYS. *Traité d'Hydraulique Environnementale*, Vol. 9 of, 115–134.

Bouvier, C., N. Chahinian, M. Adamovic, C. Cassé, A. Crespy, A. Crès, and M. Alcoba, 2017: Large-Scale GIS-Based Urban Flood Modelling: A Case Study on the City of Ouagadougou. *Advances in Hydroinformatics*, P. Gourbesville, J. Cunge, and G. Caignaert, Eds., *Springer Water*, Springer Singapore, 703–717.

——, and Coauthors, 2018: Modélisation à fine résolution spatiale des inondations dans une agglomération urbaine, par couplage d'une modèle hydrologique et d'un modèle de transfert en réseau. *Rev. Int. L'eau*, 10.

Bradshaw, C. J. A., N. S. Sodhi, K. S. H. Peh, and B. W. Brook, 2007: Global evidence that deforestation amplifies flood risk and severity in the developing world. *Glob. Change Biol.*, **13**, 2379–2395, https://doi.org/10.1111/j.1365-2486.2007.01446.x.

Brauer, C. C., A. Overeem, H. Leijnse, and R. Uijlenhoet, 2016: The effect of differences between rainfall measurement techniques on groundwater and discharge simulations in a lowland catchment: Rainfall Measurement Techniques for Hydrological Simulations. *Hydrol. Process.*, **30**, 3885–3900, https://doi.org/10.1002/hyp.10898.

Cecinati, F., A. de Niet, K. Sawicka, and M. Rico-Ramirez, 2017: Optimal Temporal Resolution of Rainfall for Urban Applications and Uncertainty Propagation. *Water*, **9**, 25, https://doi.org/10.3390/w9100762.

Chwala, C., and H. Kunstmann, 2019: Commercial microwave link networks for rainfall observation: Assessment of the current status and future challenges. *Wiley Interdiscip. Rev. Water*, **6**, 20, https://doi.org/10.1002/wat2.1337.

——, ——, S. Hipp, and U. Siart, 2014: A monostatic microwave transmission experiment for line integrated precipitation and humidity remote sensing. *Atmospheric Res.*, **144**, 57–72, https://doi.org/10.1016/j.atmosres.2013.05.014.

——, F. Keis, and H. Kunstmann, 2016: Real-time data acquisition of commercial microwave link networks for hydrometeorological applications. *Atmospheric Meas. Tech.*, **9**, 991–999, https://doi.org/10.5194/amt-9-991-2016.

CRED, 2015: *Human Cost of Natural Disasters: A Global Perspective | EM-DAT*. CRED, https://www.emdat.be/human_cost_natdis (Accessed May 13, 2020).

D'Amico, M., A. Manzoni, and G. L. Solazzi, 2016: Use of Operational Microwave Link Measurements for the Tomographic Reconstruction of 2-D Maps of Accumulated Rainfall. *IEEE Geosci. Remote Sens. Lett.*, **13**, 1827–1831, https://doi.org/10.1109/LGRS.2016.2614326.

David, N., P. Alpert, and H. Messer, 2013: The potential of cellular network infrastructures for sudden rainfall monitoring in dry climate regions. *Atmospheric Res.*, **131**, 13–21, https://doi.org/10.1016/j.atmosres.2013.01.004.

Accepted for publication in *Journal of Hydrometeorology*. DOI 10.1175/JHM-D-20-0163.1.

675 Depraetere, C., M. Gosset, S. Ploix, and H. Laurent, 2009: The organization and kinematics
676 of tropical rainfall systems ground tracked at mesoscale with gages: First results from
677 the campaigns 1999–2006 on the Upper Ouémé Valley (Benin). *J. Hydrol.*, **375**, 143–
678 160, https://doi.org/10.1016/j.jhydrol.2009.01.011.

679 Dieulin, C., G. Mahé, J.-E. Paturel, S. Ejjiyar, Y. Tramblay, N. Rouché, and B. EL Mansouri,
680 2019: A New 60-year 1940/1999 Monthly-Gridded Rainfall Data Set for Africa.
681 *Water*, **11**, 387, https://doi.org/10.3390/w11020387.

682 Doumounia, A., M. Gosset, F. Cazenave, M. Kacou, and F. Zougmore, 2014: Rainfall
683 monitoring based on microwave links from cellular telecommunication networks: First
684 results from a West African test bed: WIRELESS NETWORKS FOR RAINFALL IN
685 AFRICA. *Geophys. Res. Lett.*, **41**, 6016–6022,
686 https://doi.org/10.1002/2014GL060724.

687 Ebi, K. L., and K. Bowen, 2016: Extreme events as sources of health vulnerability: Drought
688 as an example. *Weather Clim. Extrem.*, **11**, 95–102,
689 https://doi.org/10.1016/j.wace.2015.10.001.

690 Egbinola, C. N., H. D. Olaniran, and A. C. Amanambu, 2017: Flood management in cities of
691 developing countries: the example of Ibadan, Nigeria: Flood management in
692 developing countries. *J. Flood Risk Manag.*, **10**, 546–554,
693 https://doi.org/10.1111/jfr3.12157.

694 Engel, T., A. H. Fink, P. Knippertz, G. Pante, and J. Bliefernicht, 2017: Extreme Precipitation
695 in the West African Cities of Dakar and Ouagadougou: Atmospheric Dynamics and
696 Implications for Flood Risk Assessments. *J. Hydrometeorol.*, **18**, 2937–2957,
697 https://doi.org/10.1175/JHM-D-16-0218.1.

698 Fencl, M., and V. Bares, 2019: Rainfall retrieval from E-band commercial microwave links.
699 *Geophys. Res. Abstr.*, **21**, 1.

700 Fencl, M., J. Rieckermann, M. Schleiss, D. Stránský, and V. Bareš, 2013: Assessing the
701 potential of using telecommunication microwave links in urban drainage modelling.
702 *Water Sci. Technol.*, **68**, 1810–1818, https://doi.org/10.2166/wst.2013.429.

703 Fencl, M., J. Rieckermann, P. Sýkora, D. Stránský, and V. Bareš, 2015: Commercial
704 microwave links instead of rain gauges: fiction or reality? *Water Sci. Technol.*, **71**, 31–
705 37, https://doi.org/10.2166/wst.2014.466.

706 ——, M. Dohnal, J. Rieckermann, and V. Bareš, 2017: Gauge-adjusted rainfall estimates
707 from commercial microwave links. *Hydrol. Earth Syst. Sci.*, **21**, 617–634,
708 https://doi.org/10.5194/hess-21-617-2017.

709 Fenicia, F., L. Pfister, D. Kavetski, P. Matgen, J.-F. Iffly, L. Hoffmann, and R. Uijlenhoet,
710 2012: Microwave links for rainfall estimation in an urban environment: Insights from
711 an experimental setup in Luxembourg-City. *J. Hydrol.*, **464–465**, 69–78,
712 https://doi.org/10.1016/j.jhydrol.2012.06.047.

713 Gosset, M., and Coauthors, 2016: Improving Rainfall Measurement in Gauge Poor Regions
714 Thanks to Mobile Telecommunication Networks. *Bull. Am. Meteorol. Soc.*, **97**, ES49–
715 ES51, https://doi.org/10.1175/BAMS-D-15-00164.1.

Accepted for publication in *Journal of Hydrometeorology*. DOI 10.1175/JHM-D-20-0163.1.

716 ——, M. Alcoba, R. Roca, S. Cloché, and G. Urbani, 2018: Evaluation of TAPEER daily
717 estimates and other GPM- era products against dense gauge networks in West Africa,
718 analysing ground reference uncertainty. *Q. J. R. Meteorol. Soc.*, **144**, 255–269,
719 https://doi.org/10.1002/qj.3335.

720 Graf, M., C. Chwala, J. Polz, and H. Kunstmann, 2020: Rainfall estimation from a German-
721 wide commercial microwave link network: optimized processing and validation for 1
722 year of data. *Hydrol. Earth Syst. Sci.*, **24**, 2931–2950, https://doi.org/10.5194/hess-24-
723 2931-2020.

724 Guilloteau, C., R. Roca, M. Gosset, and V. Venugopal, 2018: Stochastic generation of
725 precipitation fraction at high resolution with a multiscale constraint from satellite
726 observations. *Q. J. R. Meteorol. Soc.*, **144**, 176–190, https://doi.org/10.1002/qj.3314.

727 Gupta, H. V., H. Kling, K. K. Yilmaz, and G. F. Martinez, 2009: Decomposition of the mean
728 squared error and NSE performance criteria: Implications for improving hydrological
729 modelling. *J. Hydrol.*, **377**, 80–91, https://doi.org/10.1016/j.jhydrol.2009.08.003.

730 Hoedjes, J., and Coauthors, 2014: A Conceptual Flash Flood Early Warning System for
731 Africa, Based on Terrestrial Microwave Links and Flash Flood Guidance. *ISPRS Int.*
732 *J. Geo-Inf.*, **3**, 584–598, https://doi.org/10.3390/ijgi3020584.

733 Islam, M. R., and A. R. Tharek, 2000: Measurement of wet antenna effect on microwave
734 propagation at 23, 26 and 38 GHz. *IEEE Antennas and Propagation Society*
735 *International Symposium. Transmitting Waves of Progress to the Next Millennium.*
736 *2000 Digest. Held in conjunction with: USNC/URSI National Radio Science Meeting*
737 *(Cat. No.00CH37118)*, Vol. 4 of, IEEE Antennas and Propagation Society
738 International Symposium. Transmitting Waves of Progress to the Next Millennium,
739 Salt Lake City, UT, USA, IEEE, 2094–2098.

740 ITU, 2004: *African Telecommunication Indicators*. 140 pp.

741 Kacou, M., 2014: Analyse des précipitations en zone sahélienne à partir d'un radar bande X
742 polarimétrique. Université Paul Sabatier et Université Félix Houphouët-Boigny, 225
743 pp.

744 Kharadly, M. M. Z., and R. Ross, 2001: Effect of wet antenna attenuation on propagation data
745 statistics. *IEEE Trans. Antennas Propag.*, **49**, 1183–1191,
746 https://doi.org/10.1109/8.943313.

747 Kim, M.-S., and B. Kwon, 2018: Rainfall Detection and Rainfall Rate Estimation Using
748 Microwave Attenuation. *Atmosphere*, **9**, 21, https://doi.org/10.3390/atmos9080287.

749 Koffi, A. K., M. Gosset, E.-P. Zahiri, A. D. Ochou, M. Kacou, F. Cazenave, and P. Assamoi,
750 2014: Evaluation of X-band polarimetric radar estimation of rainfall and rain drop size
751 distribution parameters in West Africa. *Atmospheric Res.*, **143**, 438–461,
752 https://doi.org/10.1016/j.atmosres.2014.03.009.

753 Kovacs, Y., N. Doussin, and M. Gaussens, 2017: *Flood risk and cities in developing*
754 *countries*. AFD, SEPIA Conseils,
755 https://www.pseau.org/outils/ouvrages/afd_flood_risk_and_cities_in_developing_cou
756 ntries_en_2017.pdf (Accessed May 13, 2020).

Accepted for publication in *Journal of Hydrometeorology*. DOI 10.1175/JHM-D-20-0163.1.

757 Leijnse, H., R. Uijlenhoet, and J. N. M. Stricker, 2007a: Hydrometeorological application of a
758 microwave link: 2. Precipitation. *Water Resour. Res.*, **43**, 9,
759 https://doi.org/10.1029/2006WR004989.

760 ——, ——, and ——, 2007b: Rainfall measurement using radio links from cellular
761 communication networks: RAPID COMMUNICATION. *Water Resour. Res.*, **43**, 6,
762 https://doi.org/10.1029/2006WR005631.

763 Leijnse, H., R. Uijlenhoet, and I. Holleman, 2008a: Sources of error in microwave link
764 rainfall estimation. Proceedings of the International Symposium on Weather Radar
765 and Hydrology, Grenoble, 4.

766 Leijnse, H., R. Uijlenhoet, and J. N. M. Stricker, 2008b: Microwave link rainfall estimation:
767 Effects of link length and frequency, temporal sampling, power resolution, and wet
768 antenna attenuation. *Adv. Water Resour.*, **31**, 1481–1493,
769 https://doi.org/10.1016/j.advwatres.2008.03.004.

770 Leijnse, H., R. Uijlenhoet, and A. Berne, 2010: Errors and Uncertainties in Microwave Link
771 Rainfall Estimation Explored Using Drop Size Measurements and High-Resolution
772 Radar Data. *J. Hydrometeorol.*, **11**, 1330–1344,
773 https://doi.org/10.1175/2010JHM1243.1.

774 Matrosov, S. Y., 2010: Evaluating Polarimetric X-Band Radar Rainfall Estimators during
775 HMT. *J. Atmospheric Ocean. Technol.*, **27**, 122–134,
776 https://doi.org/10.1175/2009JTECHA1318.1.

777 Messer, H., A. Zinevich, and P. Alpert, 2006: Environmental Monitoring by Wireless
778 Communication Networks. *Science*, **312**, 713–713,
779 https://doi.org/10.1126/science.1120034.

780 Mie, G., 1908: Beiträge zur Optik trüber Medien, speziell kolloidaler Metallösungen. *Ann.*
781 *Phys.*, **330**, 377–445, https://doi.org/10.1002/andp.19083300302.

782 Moumouni, S., M. Gosset, and E. Houngninou, 2008: Main features of rain drop size
783 distributions observed in Benin, West Africa, with optical disdrometers. *Geophys. Res.*
784 *Lett.*, **35**, L23807, https://doi.org/10.1029/2008GL035755.

785 Nikulin, G., and Coauthors, 2018: The effects of 1.5 and 2 degrees of global warming on
786 Africa in the CORDEX ensemble. *Environ. Res. Lett.*, **13**, 11,
787 https://doi.org/10.1088/1748-9326/aab1b1.

788 Noam, E. M., 1999: *Telecommunications in Africa*. Oxfort University Press. 305 pp.

789 Novella, N. S., and W. M. Thiaw, 2013: African Rainfall Climatology Version 2 for Famine
790 Early Warning Systems. *J. Appl. Meteorol. Climatol.*, **52**, 588–606,
791 https://doi.org/10.1175/JAMC-D-11-0238.1.

792 Ostrometzky, J., and A. Eshel, 2018: Empirical Study of the Quantization Induced Bias in
793 Commercial Microwave Links' Min/Max Attenuation Measurements for Rain
794 Monitoring. *Environments*, **5**, 9, https://doi.org/10.3390/environments5070080.

Accepted for publication in *Journal of Hydrometeorology*. DOI 10.1175/JHM-D-20-0163.1.

795 Overeem, A., H. Leijnse, and R. Uijlenhoet, 2011: Measuring urban rainfall using microwave
796 links from commercial cellular communication networks: MEASURING URBAN
797 RAINFALL USING MICROWAVE LINKS. *Water Resour. Res.*, **47**, 1–16,
798 https://doi.org/10.1029/2010WR010350.

799 ——, ——, and ——, 2013: Country-wide rainfall maps from cellular communication
800 networks. *Proc. Natl. Acad. Sci.*, **110**, 2741–2745,
801 https://doi.org/10.1073/pnas.1217961110.

802 Overeem, A., H. Leijnse, and R. Uijlenhoet, 2016a: Retrieval algorithm for rainfall mapping
803 from microwave links in a cellular communication network. *Atmospheric Meas. Tech.*,
804 **9**, 2425–2444, https://doi.org/10.5194/amt-9-2425-2016.

805 Overeem, A., H. Leijnse, and R. Uijlenhoet, 2016b: Two and a half years of country-wide
806 rainfall maps using radio links from commercial cellular telecommunication networks:
807 TWO AND A HALF YEARS OF RADIO LINK RAINFALL MAPS. *Water Resour.*
808 *Res.*, **52**, 8039–8065, https://doi.org/10.1002/2016WR019412.

809 Pastorek, J., M. Fencl, J. Rieckermann, and V. Bareš, 2019: Commercial microwave links for
810 urban drainage modelling: The effect of link characteristics and their position on
811 runoff simulations. *J. Environ. Manage.*, **251**, 109522,
812 https://doi.org/10.1016/j.jenvman.2019.109522.

813 Polz, J., C. Chwala, M. Graf, and H. Kunstmann, 2020: Rain event detection in commercial
814 microwave link attenuation data using convolutional neural networks. *Atmospheric*
815 *Meas. Tech.*, 22, https://doi.org/10.5194/amt-2019-412.

816 Rios Gaona, M. F., A. Overeem, T. H. Raupach, H. Leijnse, and R. Uijlenhoet, 2017: Rainfall
817 retrieval with commercial microwave links in São Paulo, Brazil. *Atmospheric Meas.*
818 *Tech.*, **11**, 4465–4476, https://doi.org/10.5194/amt-11-4465-2018.

819 Roversi, G., P. P. Alberoni, A. Fornasiero, and F. Porcù, 2020: Commercial microwave links
820 as a tool for operational rainfall monitoring in Northern Italy. *Atmospheric Meas.*
821 *Tech.*, **13**, 5779–5797, https://doi.org/10.5194/amt-13-5779-2020.

822 Schleiss, M., and A. Berne, 2010: Identification of Dry and Rainy Periods Using
823 Telecommunication Microwave Links. *IEEE Geosci. Remote Sens. Lett.*, **7**, 611–615,
824 https://doi.org/10.1109/LGRS.2010.2043052.

825 ——, J. Rieckermann, and A. Berne, 2013: Quantification and Modeling of Wet-Antenna
826 Attenuation for Commercial Microwave Links. *IEEE Geosci. Remote Sens. Lett.*, **10**,
827 1195–1199, https://doi.org/10.1109/LGRS.2012.2236074.

828 Smiatek, G., F. Keis, C. Chwala, B. Fersch, and H. Kunstmann, 2017: Potential of
829 commercial microwave link network derived rainfall for river runoff simulations.
830 *Environ. Res. Lett.*, **12**, 034026, https://doi.org/10.1088/1748-9326/aa5f46.

831 Sohail Afzal, M., S. H. H. Shah, M. J. M. Cheema, and R. Ahmad, 2018: Real time rainfall
832 estimation using microwave signals of cellular communication networks: a case study
833 of Faisalabad, Pakistan. *Hydrol. Earth Syst. Sci. Discuss.*, 1–20,
834 https://doi.org/10.5194/hess-2017-740.

Accepted for publication in *Journal of Hydrometeorology*. DOI 10.1175/JHM-D-20-0163.1.

Stransky, D., M. Fencl, and V. Bares, 2018: Runoff prediction using rainfall data from microwave links: Tabor case study. *Water Sci. Technol.*, **2017**, 351–359, https://doi.org/10.2166/wst.2018.149.

Thiessen, A. H., 1911: Climatological data for july, 1911 - District No. 10, Great basin. *Mon. WEATHER Rev.*, 1082–1084.

Uijlenhoet, R., A. Overeem, and H. Leijnse, 2018: Opportunistic remote sensing of rainfall using microwave links from cellular communication networks. *Wiley Interdiscip. Rev. Water*, **5**, 1–15, https://doi.org/10.1002/wat2.1289.

de Vos, L. W., A. Overeem, H. Leijnse, and R. Uijlenhoet, 2019: Rainfall Estimation Accuracy of a Nationwide Instantaneously Sampling Commercial Microwave Link Network: Error Dependency on Known Characteristics. *J. Atmospheric Ocean. Technol.*, **36**, 1267–1283, https://doi.org/10.1175/JTECH-D-18-0197.1.

Zinevich, A., P. Alpert, and H. Messer, 2008: Estimation of rainfall fields using commercial microwave communication networks of variable density. *Adv. Water Resour.*, **31**, 1470–1480, https://doi.org/10.1016/j.advwatres.2008.03.003.

——, H. Messer, and P. Alpert, 2009: Frontal Rainfall Observation by a Commercial Microwave Communication Network. *J. Appl. Meteorol. Climatol.*, **48**, 1317–1334, https://doi.org/10.1175/2008JAMC2014.1.

Zinevich, A., H. Messer, and P. Alpert, 2010: Prediction of rainfall intensity measurement errors using commercial microwave communication links. *Atmospheric Meas. Tech.*, **3**, 1385–1402, https://doi.org/10.5194/amt-3-1385-2010.

Zohidov, B., H. Andrieu, M. Servières, and N. Normand, 2016: Retrieval of rainfall fields in urban areas using attenuation measurements from mobile phone networks: a modeling feasibility study. *Hydrol. Earth Syst. Sci. Discuss.*, 1–30, https://doi.org/10.5194/hess-2016-540.

Accepted for publication in *Journal of Hydrometeorology*. DOI 10.1175/JHM-D-20-0163.1.

Tables

Frequency (GHz)		6	12	18	24	30
(a ; b)		(0.00145 ; 1.29)	(0.0268 ; 1.17)	(0.0818 ; 1.06)	(0.143 ; 1.03)	(0.226 ; 0.997)
Rainfall equivalent PIA/L (mm/h)	1dB/1km	*157*	22.1	10.6	6.57	4.447
	0.1dB/1km 1dB/10km	26.4	3.08	1.21	0.705	0.442
	0.1dB/10km	4.46	0.430	0.137	*0.0756*	*0.0439*

Table 1:

Minimum detectable rainfall ($mm.h^{-1}$) as a function of frequency, signal precision and link length.

The second row reports the values of the prefactor (*a*) and exponent (*b*) of the attenuation-rainfall or k-R relationship (see text) for the indicated frequencies. The three last rows illustrate the equivalent in rain rate [mm/h], of an increment in the measured attenuation (0.1 or 1 dB) for the indicated link length (1 km, 10 km) and frequency. The *italic* highlights frequency/length combinations which are not likely on operational networks (short link and low frequency ; long link at high frequency).

Accepted for publication in *Journal of Hydrometeorology*. DOI 10.1175/JHM-D-20-0163.1.

	Bias abs (%)		Err max abs (%)		KGE	
	1060	1074	1060	1074	1060	1074
Radar mean	37.6	47.6	60.1	50.8	0.19	0.60
One pixel	26.7	75.4	55.0	83.6	0.24	0.71
Perfect	8.80	7.07	17.1	7.27	0.77	0.90
0.1 dB	8.83	6.23	17.9	7.04	0.76	0.91
1 dB	12.0	4.43	23.8	8.68	0.71	0.91

Table 2 :

Statistics on the simulated discharge for different rainfall sampling experiments compared to the reference simulation (based on the high-resolution rain map). The following statistics are reported for the two main outlets (1060 and 1074, see text) : the absolute error on the event mean discharge (in %) ; the absolute error on the event maximum discharge (in %) ; the KGE. For each statistics the mean over the 3 events is reported. The scores are reported for the following rainfall forcing as described in section 5c: spatial mean of radar rainfall ; rainfall at central pixel ; rainfall from the 75 links at 13 Ghz network (Fig. 1) with perfect precision, precision 0.1 dB or precision 1 dB.

Accepted for publication in *Journal of Hydrometeorology*. DOI 10.1175/JHM-D-20-0163.1.

900

901

902 **Figures**

903

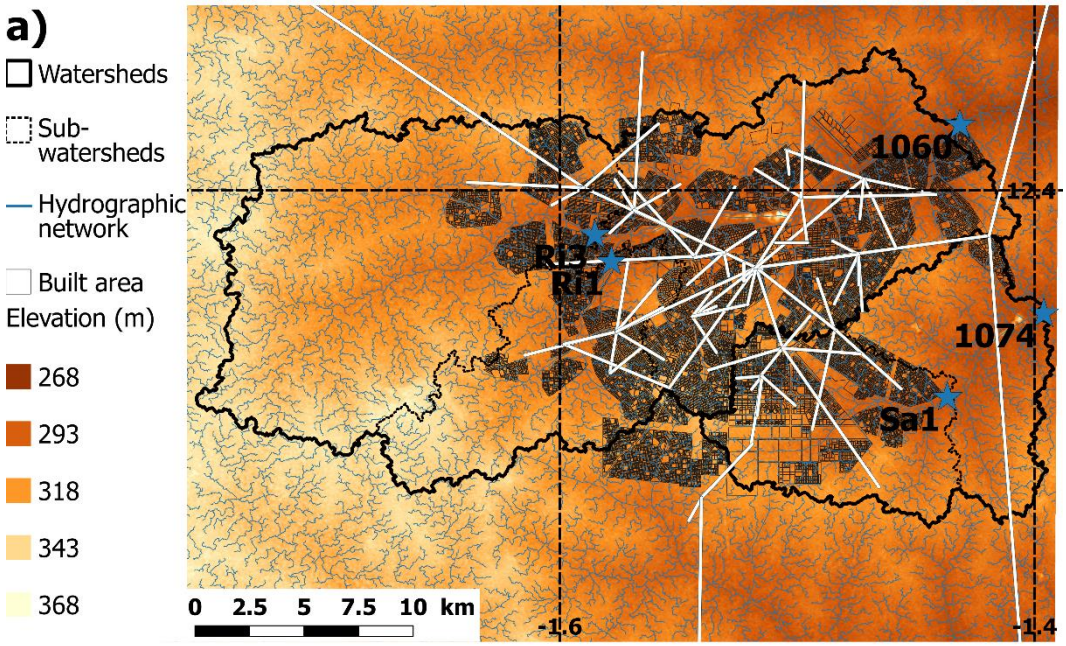

904

905

906 Figure 1 : The study area in Ouagadougou. The gray shading is the urbanized (built) area ; the
907 blue lines represent the hydrographic network and the black lines the contours of the studied
908 basins and sub-basins ; the blue stars are the outlets where the simulated discharge is analyzed
909 for the various numerical experiments detailed in the text. The white lines are the positions of
910 the 75 microwave-links (13 GHz) available for one of the operational mobile networks.

911

912

913

914

Accepted for publication in *Journal of Hydrometeorology*. DOI 10.1175/JHM-D-20-0163.1.

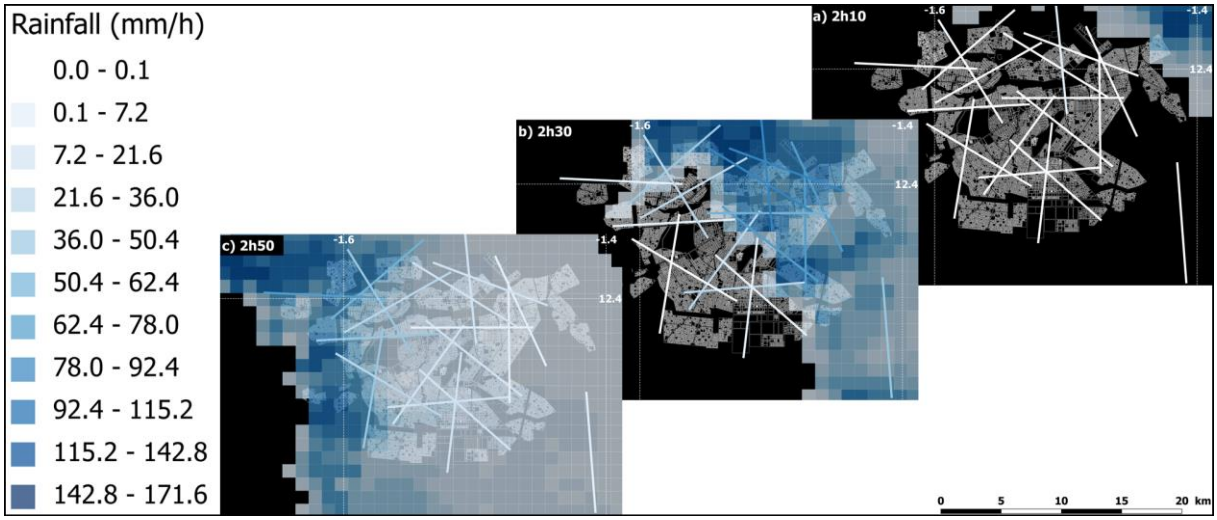

Fig 2 :

Figure 2 : Evolution of rain intensity maps over the area on the 2012/08/04 event as seen by the radar and the simulated links. The three images show the radar rain maps crossing the study domain at three moments in time a) 02:10 UTC. b) 02:30 UTC and c) 02:50 UTC; the color shading over the 1kmx1km pixels show the rainfall intensity as indicated by the legend. The nineteen straight lines superimposed on each image represent the simulated microwave links and their color indicates the mean rainfall over the link, as calculated by the link simulator (see text and Eq 5.).

Accepted for publication in *Journal of Hydrometeorology*. DOI 10.1175/JHM-D-20-0163.1.

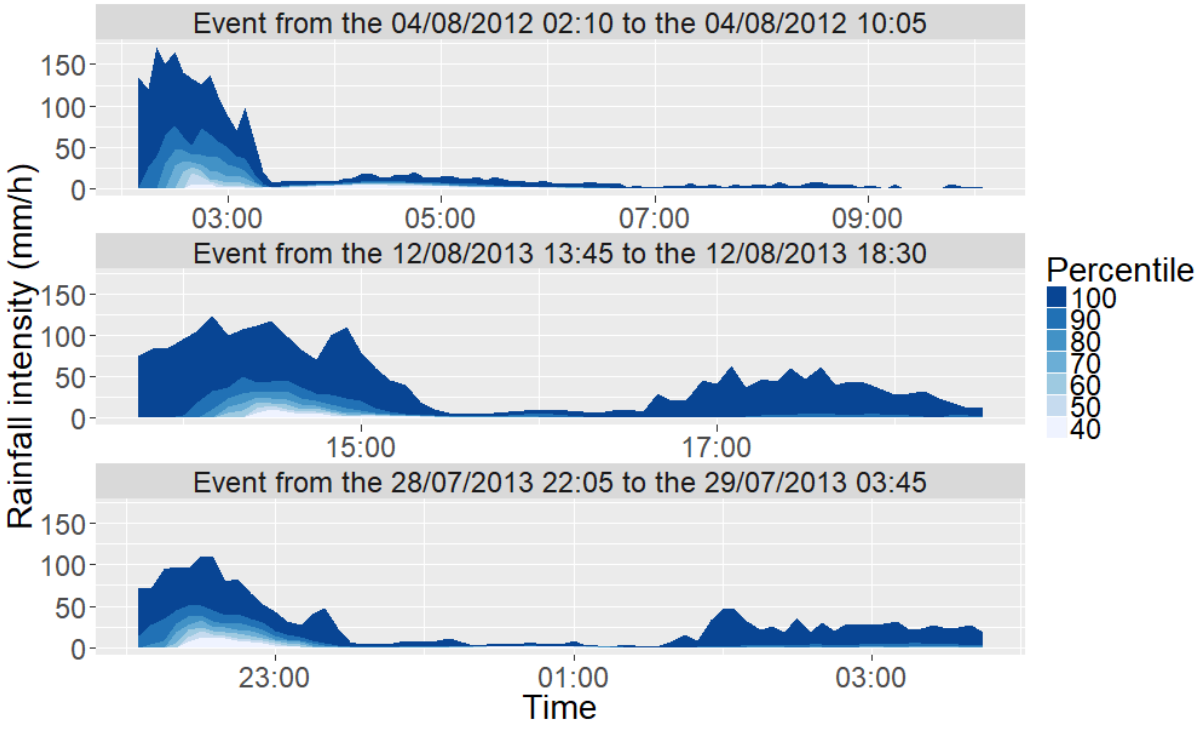

Figure 3: Time evolution of radar rainfall over the studied area (from Fig. 1) for the three indicated rainfall events. For each five minutes time step the distribution of the rainfall rates among the 1060 radar pixels is illustrated by the percentiles.

Accepted for publication in *Journal of Hydrometeorology*. DOI 10.1175/JHM-D-20-0163.1.

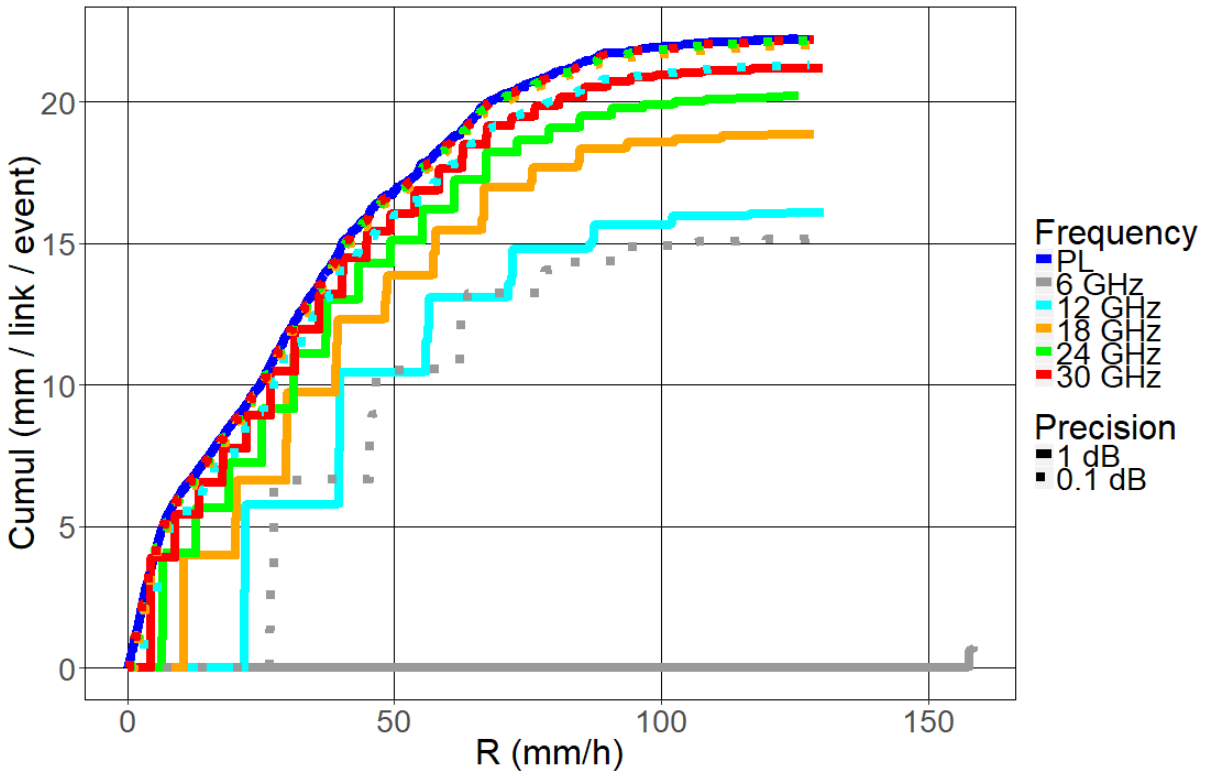

Figure 4: Cumulated rainfall distribution per rain rate classes as a function of link frequency and attenuation precision – here for links of length 1 km. The Y axis is the mean amount of rainfall per link and event (see text) and the X axis the intensity classes. The dark blue line is for a link with perfect precision; for the others the color indicates the frequency (GHz), the plain lines are for precision 1dB and the dash line for precision 0.1 dB.

Accepted for publication in *Journal of Hydrometeorology*. DOI 10.1175/JHM-D-20-0163.1.

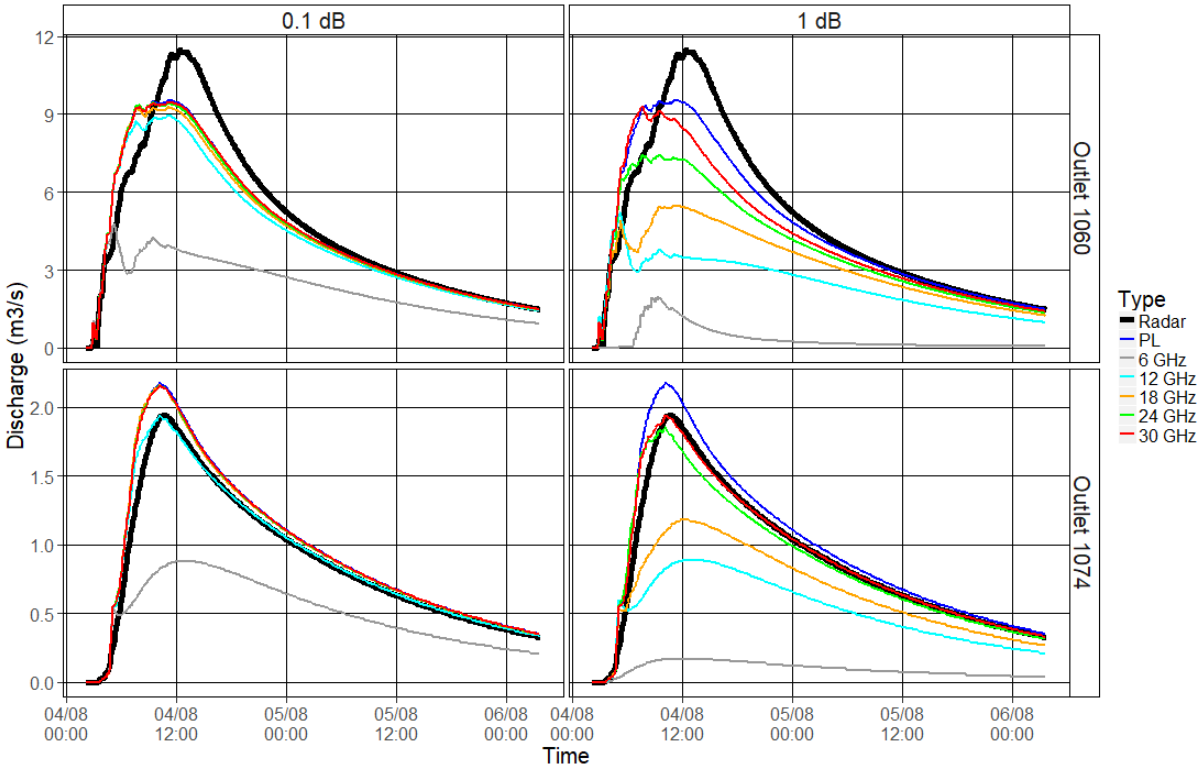

965

966

967

968 Figure 5: Effect of raw signal precision for different frequencies on the simulated discharge for
969 the 2020/08/04 event (top row in Fig. 3). The top figures are for outlet 1060 and the bottom
970 figures for outlet 1074. The left column is for precision 0.1 dB and the right column for 1 dB.
971 As for Figure 4 the length is 1 km for all links and their frequency is indicated by the color. The
972 dark blue line is for links with perfect precision and the black line is for the reference simulation
973 based on the high-resolution radar map.

974

975

976

977

Accepted for publication in *Journal of Hydrometeorology*. DOI 10.1175/JHM-D-20-0163.1.

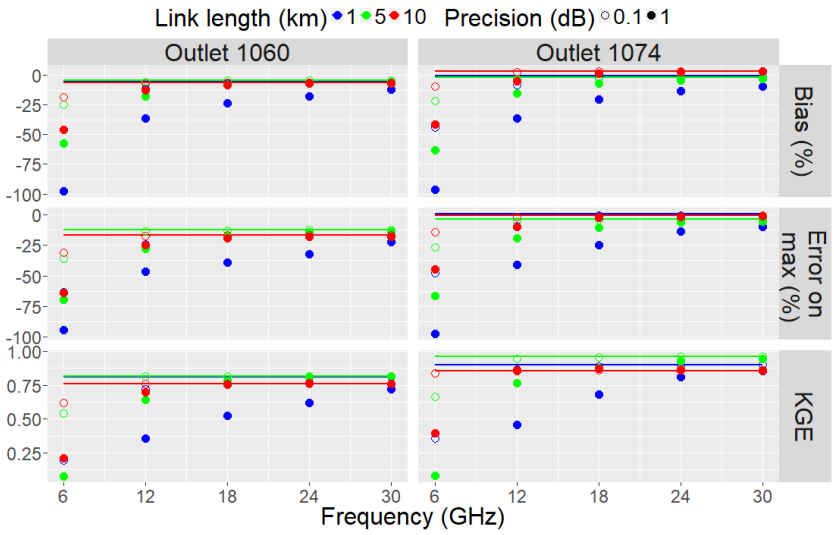

Figure 6: Effect of signal precision, link length and frequency on the simulated discharge. The simulated discharge when the model is forced by microwave links (with positions as in Fig. 1) is compared with the reference simulation based on the radar maps. Three criteria are presented: the mean bias on the event's discharge, the error on the maximum discharge and the KGE. For each criteria the average value for the 3 events is plotted. The left column if for outlet 1060 and the right column for outlet 1074. The results are shown as a function frequency (X axis) ; link length (blue for 1 km, green for 5, and red for 10 km) ; signal precision (hollow circles for 0.1 dB and plain dots for 1 dB). The results for the links with perfect precision are shown by the horizontal lines.

Accepted for publication in *Journal of Hydrometeorology*. DOI 10.1175/JHM-D-20-0163.1.

997

998

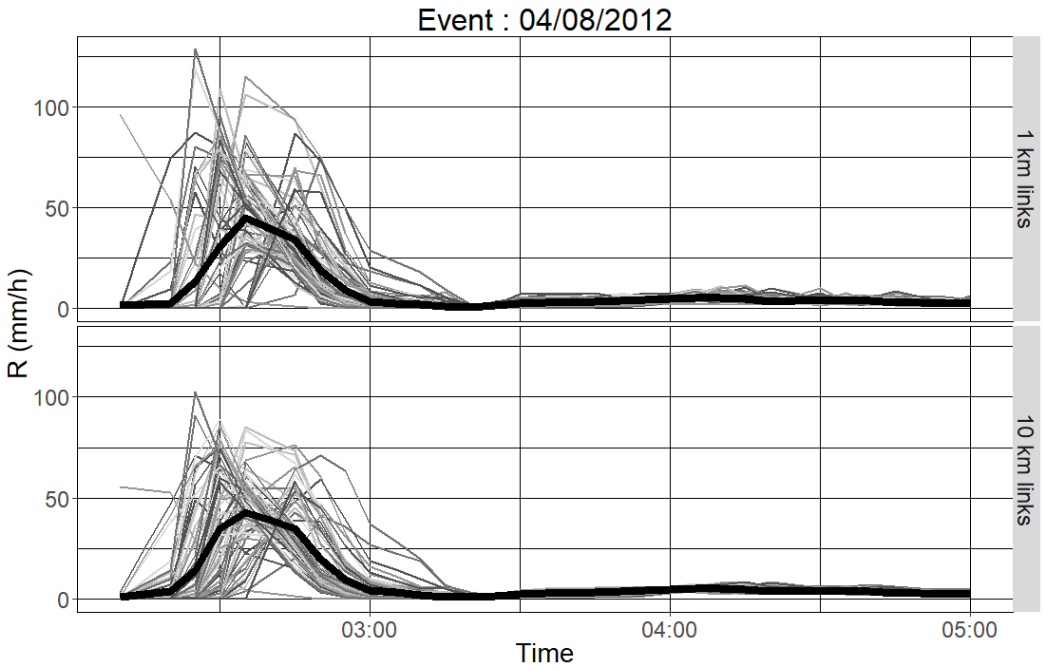

999

1000

1001

1002

1003

1004 Fig 7: Illustration of the spread within the rainfall time series among all 75 links (center position

1005 and orientation as in Fig. 1) for links of length 1 km (top) or 10 km (bottom) for the 2012/08/04

1006 event. The average rainfall over all links by 5 minutes time steps is the thick black line.

1007

1008

Accepted for publication in *Journal of Hydrometeorology*. DOI 10.1175/JHM-D-20-0163.1.

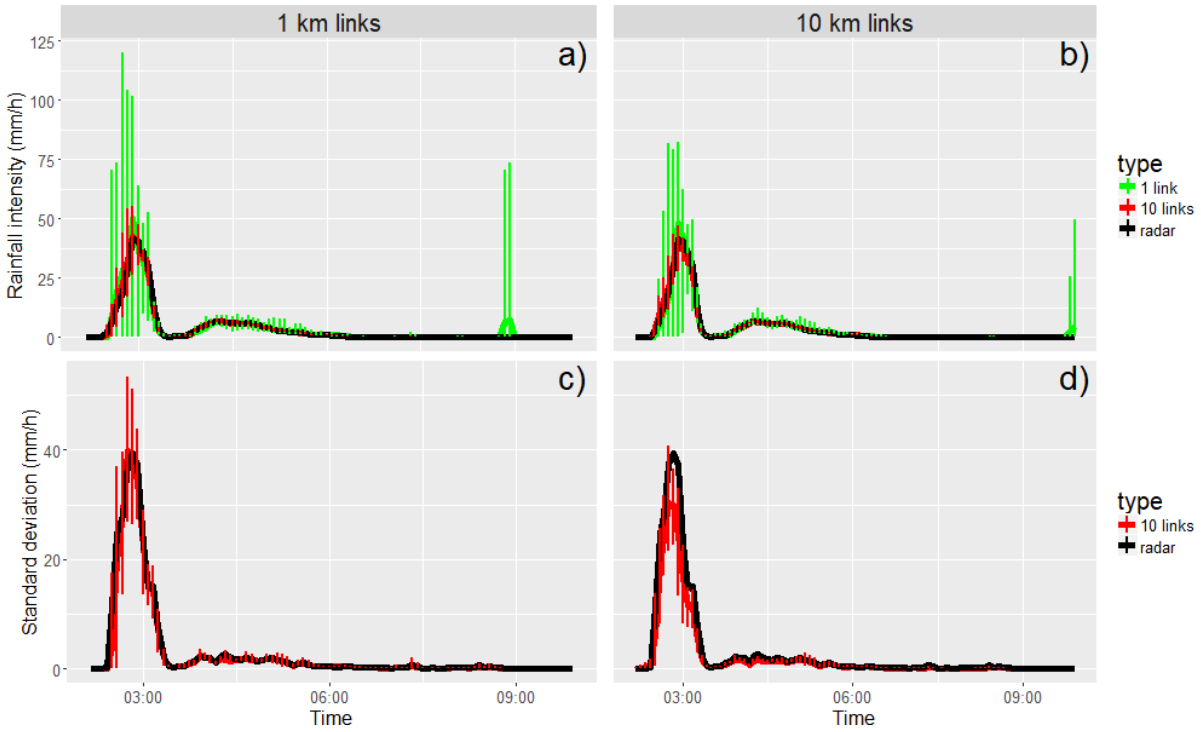

Figure 8: Rainfall variability between realizations and among simulated links, illustrated for 2012/08/04 event over the sub-basin Ri3. The top plots show the time evolution of the sub-basin average rain rate for links of size 1 km (a) or 10 km (b), in green for a network of one link and in red for a network of ten links. The links are assumed to have perfect precision. The vertical lines illustrate the spread (from minimum to maximum) among ten realizations of network simulations. The black line shows the sub-basin mean rainfall calculated from the reference radar rain field. The bottom figures show the time evolution of the standard deviation of rain rate inside the basin as captured by 10 links (red) of length 1 km (c) or 10 km(d) and by the radar (black). The vertical red lines illustrate the spread in the standard deviation (from minimum to maximum) among the ten realizations.

Accepted for publication in *Journal of Hydrometeorology*. DOI 10.1175/JHM-D-20-0163.1.

Figure 9

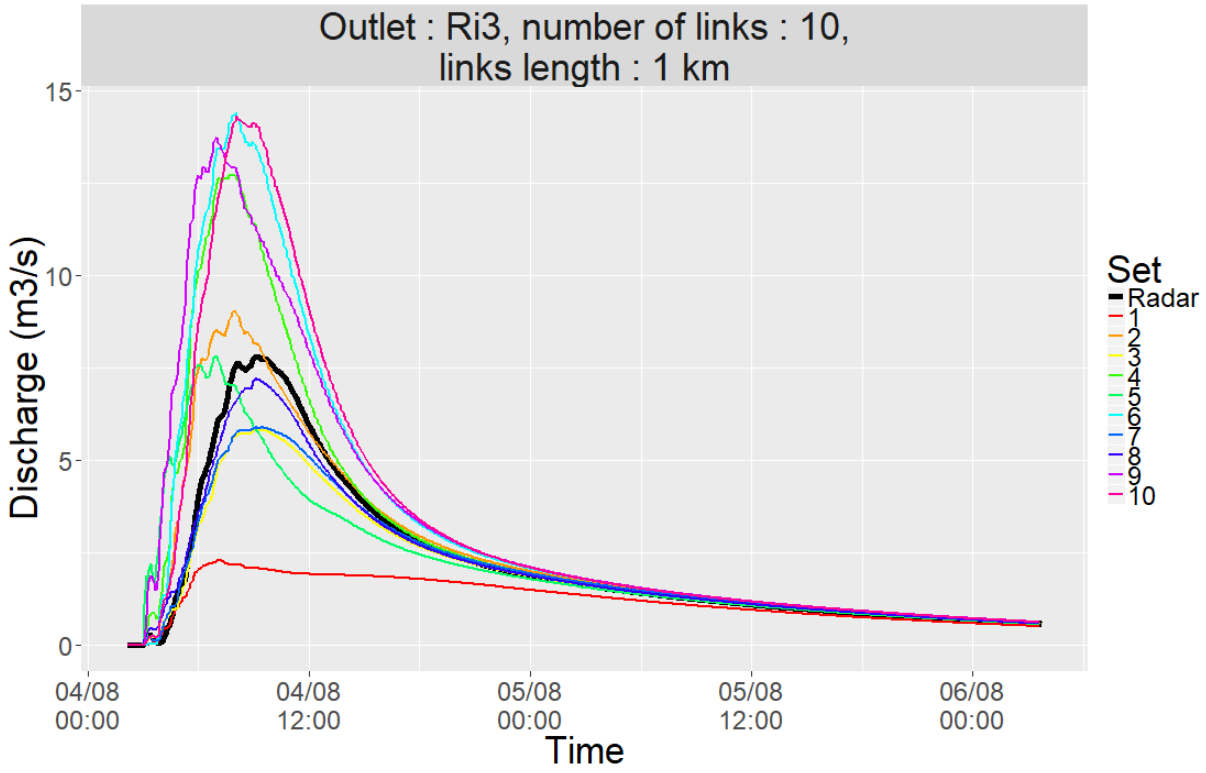

Figure 9: Simulated discharge over the Ri3 sub-basin outlet for the 2012 August 04 rainfall event, here for a simulated network of 10 links of length 1 km. The outputs for 10 realizations are displayed with different colors together with the reference simulation (black) using the radar map.

1040 Fig 10

1041

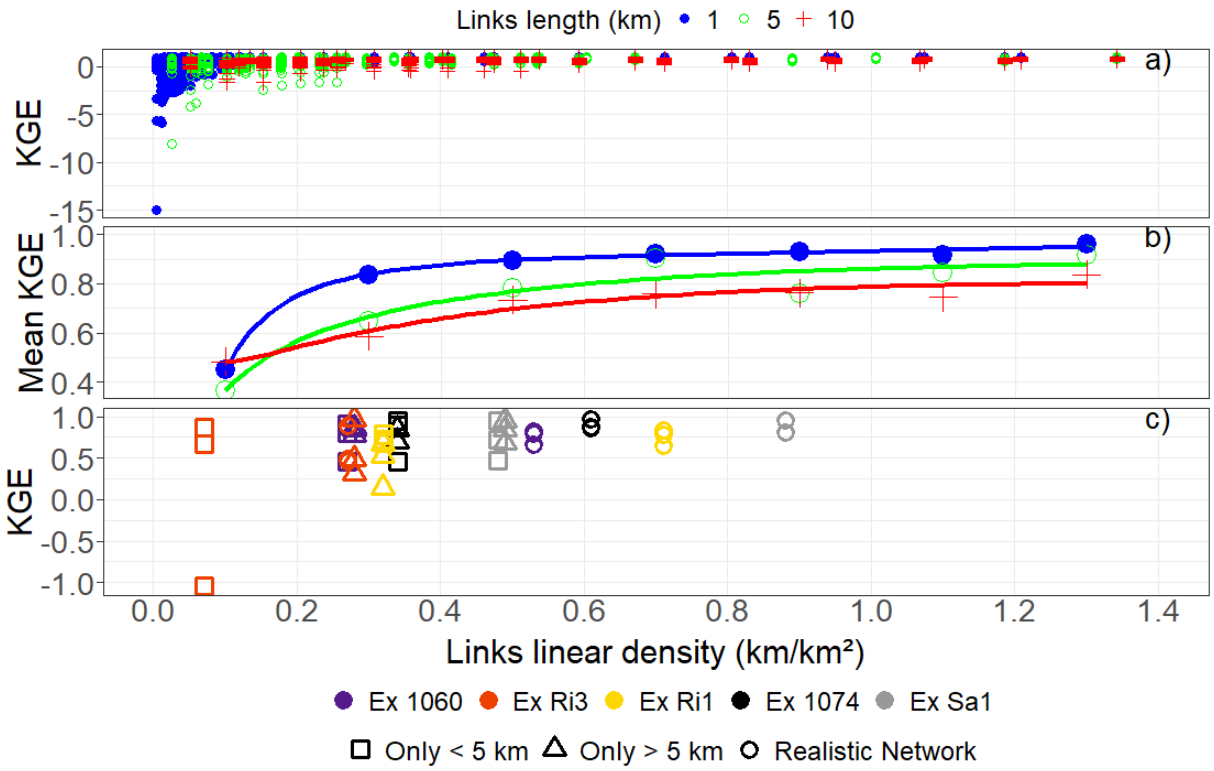

1042

1043

1044

1045 Figure 10 : Summary of the effect of rainfall sampling by the link network considering all
1046 numerical experiments : a) and b) experiments with the randomly generated network, 3 link
1047 lengths (blue dots, 1km; green circles, 5 km; red crosses, 10 km) x 10 realizations x 3 events X
1048 3 sub-basins. a) KGE for the simulated discharge compared to the reference (radar based) is
1049 shown as a point for each experiment. The X axis expresses the density of information as the
1050 cumulated length of all links inside the sub-basin (in km) per sub-basin area (in km^2). b) mean
1051 KGE per link density (average by bins of 0.2km/km^2 width). The fit on *b)* is only there for
1052 readability. c) KGE of the simulated discharge in the indicated outlets compared to the
1053 reference, for the simulations based on the actual network configuration (Fig 1), keeping the

1054 whole network (circles), keeping only links of length 5 km and below (triangles) , and keeping

1055 only links longer than 5 km .

1056

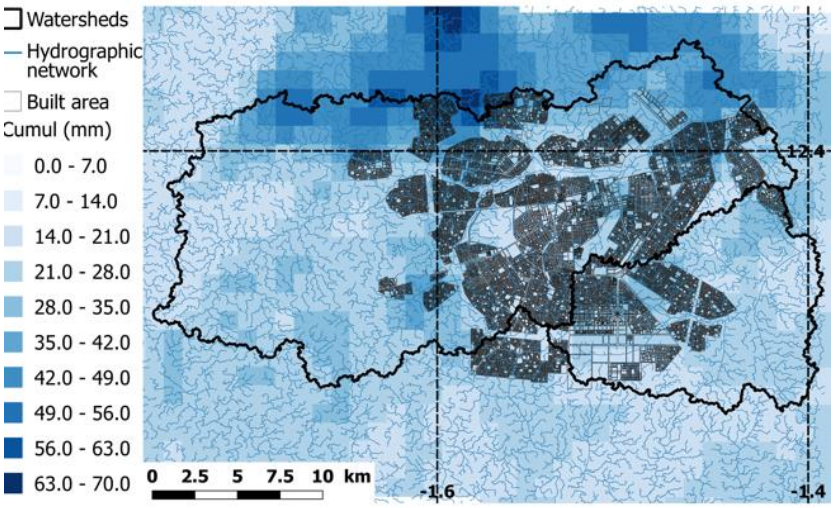

Figure 11 : rainfall accumulation map over the area for the 2012/08/04 event, as measured by the radar.

Accepted for publication in *Journal of Hydrometeorology*. DOI 10.1175/JHM-D-20-0163.1.

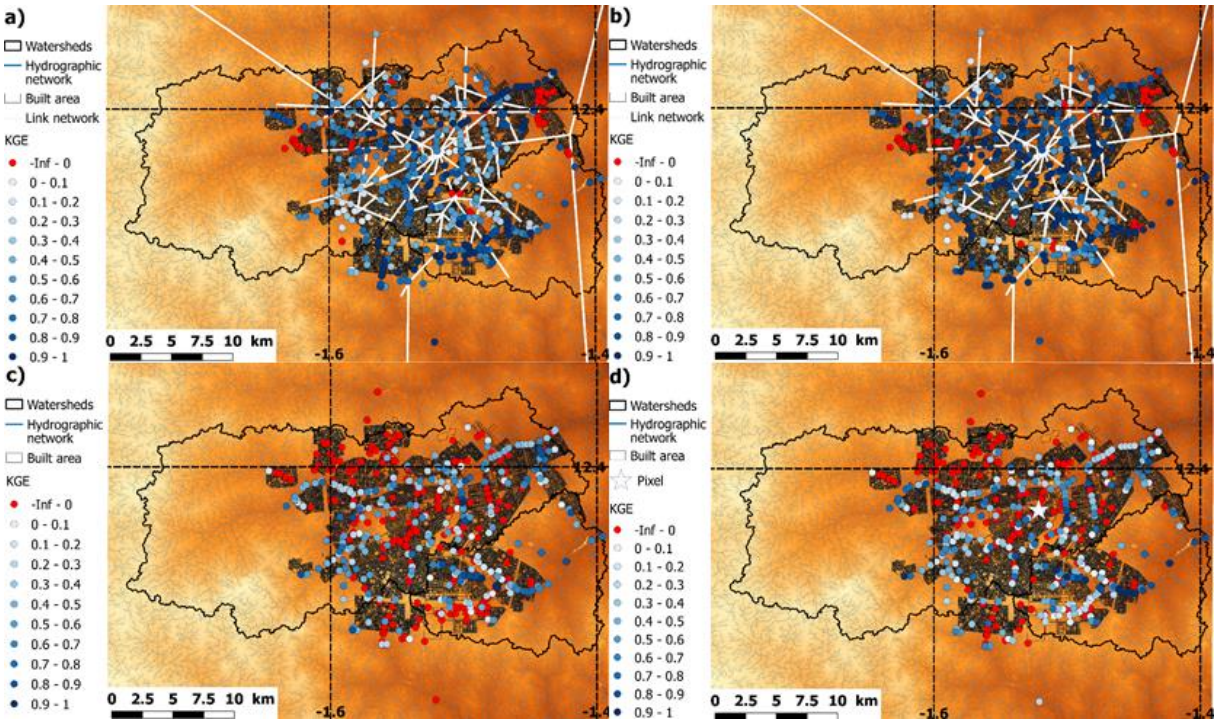

Figure 12 : Spatial distribution of KGE for the simulations with various rain forcing compared to the reference simulation based on the high resolution radar rain map, for the 2012/08/04 event : a) rain forcing based on the network seen in Fig. 1 with frequency 13 GHz and precision 1 dB b) same as *a* with precision 0.1 dB. c) rain forcing based on the area average rainfall from the radar and d) rain forcing from the central pixel (shown by a white star).

Accepted for publication in *Journal of Hydrometeorology*. DOI 10.1175/JHM-D-20-0163.1.